

Evidence from lava flows for complex polarity transitions: the new composite Steens Mountain reversal record

Nicholas A. Jarboe¹, Robert S. Coe¹ and Jonathan M.G. Glen²

¹Department of Earth and Planetary Sciences, University of California, 1156 High St., Santa Cruz, CA 95064, USA. E-mail: njarboe@gmail.com

²U.S. Geological Survey, MS989, 345 Middlefield Road, Menlo Park, CA 94025, USA

Accepted 2011 May 17. Received 2011 April 28; in original form 2010 October 2

SUMMARY

Geomagnetic polarity transitions may be significantly more complex than are currently depicted in many sedimentary and lava-flow records. By splicing together paleomagnetic results from earlier studies at Steens Mountain with those from three newly studied sections of Oregon Plateau flood basalts at Catlow Peak and Poker Jim Ridge 70–90 km to the southeast and west, respectively, we provide support for this interpretation with the most detailed account of a magnetic field reversal yet observed in volcanic rocks. Forty-five new distinguishable transitional (T) directions together with 30 earlier ones reveal a much more complex and detailed record of the 16.7 Ma reversed (R)-to-normal (N) polarity transition that marks the end of Chron C5Cr. Compared to the earlier R-T-N-T-N reversal record, the new record can be described as R-T-N-T-N-T-R-T-N. The composite record confirms earlier features, adds new west and up directions and an entire large N-T-R-T segment to the path, and fills in directions on the path between earlier directional jumps. Persistent virtual geomagnetic pole (VGP) clusters and separate VGPs have a preference for previously described longitudinal bands from transition study compilations, which suggests the presence of features at the core–mantle boundary that influence the flow of core fluid and distribution of magnetic flux. Overall the record is consistent with the generalization that VGP paths vary greatly from reversal to reversal and depend on the location of the observer. Rates of secular variation confirm that the flows comprising these sections were erupted rapidly, with maximum rates estimated to be 85–120 m ka⁻¹ at Catlow and 130–195 m ka⁻¹ at Poker Jim South. Paleomagnetic poles from other studies are combined with 32 non-transitional poles found here to give a clockwise rotation of the Oregon Plateau of 11.4° ± 5.6° with respect to the younger Columbia River Basalt Group flows to the north and 14.5° ± 4.6° with respect to cratonic North America (95 per cent confidence interval).

Key words Palaeomagnetism applied to tectonics; North America; Reversals: process, time scale, magnetostratigraphy.

1 INTRODUCTION

The Miocene Steens Basalt, which covers a large portion of the Oregon Plateau in western Oregon, USA, is best represented at the ~1000 m type section at Steens Mountain (Fuller 1931). It is the earliest eruptive unit of the Columbia River Basalt Group (CRBG) (Hooper *et al.* 2002; Camp *et al.* 2011) and is ideal for paleomagnetic study due to the large number of flows exposed. The well-exposed escarpment at Steens Mountain contains lavas that capture details of a reversal of the earth's magnetic field, as first shown by Watkins (1965). These lavas were later studied in great detail for their paleomagnetic directions (Mankinen *et al.* 1985; Camps *et al.* 1999) and their paleomagnetic intensities (Prévot *et al.* 1985), giving up till now the most detailed account recorded in

volcanic rocks of a geomagnetic polarity transition. The importance of this benchmark record is that the thermoremanence that lava flows acquire during primary cooling generally provides the most accurate spot readings of the ancient magnetic field of all natural recording media. But although volcanic sections are immune to distortions caused by delayed and non-uniform lock-in of remanence that can cause problems in sedimentary recordings, volcanic records are necessarily incomplete due to the episodic nature of volcanism (e.g. Coe & Glen 2004). Sampling other volcanic sections that erupted during the Steens reversal can reduce this incompleteness. This was first demonstrated by Camps *et al.* (1999) in their study of lavas comprising the upper half of the Steens Mountain section B, only 2 km from those that defined most of the detailed 1985 transition record (section A lavas; Mankinen *et al.* 1985). There they

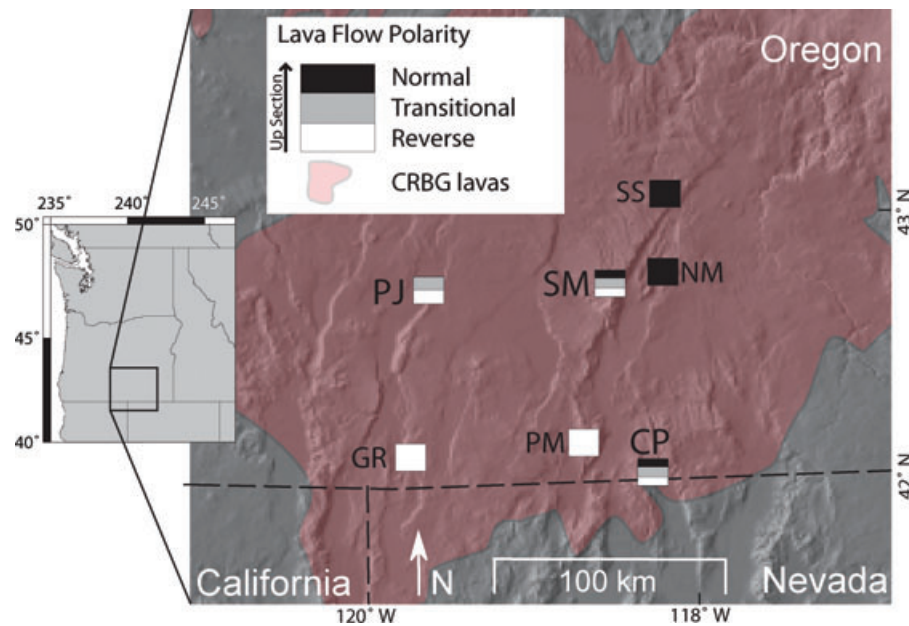


Figure 1. Location and magnetic polarity of Steens Basalt volcanic sections. CP, Catlow; GR, Guano Rim; NM, North Mickey; PJ, Poker Jim North and South; PM, Pueblo Mountains; SM, Steens Mountain; SS, Summit Springs. CP and PJ were sampled for this study. CRBG outline is from Camp & Ross (2004).

discovered two new transitional directions to add to the previous 30 directional groups, which showed that the field made a second swing to a transient normal direction during the transition. In this study, we present new results from Steens Basalt sections at three much more distant localities (Catlow, Poker Jim North and Poker Jim South) with lavas that erupted during the same transition. When combined with the directions from Steens Mountain, they give a much more complete and complex high-fidelity record than any known previously for a reversal of Earth's magnetic field.

1.1 Geologic setting

The Steens basalts are the first eruptive event in the CRBG (Hooper *et al.* 2002; Camp *et al.* 2003; Camp & Ross 2004; Hooper *et al.* 2007). This formation is among the younger large igneous provinces and covers much of eastern Washington, eastern Oregon, western Idaho and small parts of northern Nevada (Camp *et al.* 2011). The locations of the Catlow, Poker Jim North and Poker Jim South sections, which are the focus of this paper, are shown in Fig. 1. Basin and Range extension has occurred on the southern edge of the CRBG lavas, creating large escarpments up to a 1000 m or more. It is typically these steep sections that provide the best opportunities for studying polarity transitions, revealing the most complete flow-on-flow exposures. At some locations, such as at Steens and Pueblo Mountains, the bottom of the Steens basalts is exposed, but in most cases it remains covered. Recently, high-resolution $^{40}\text{Ar}/^{39}\text{Ar}$ determinations from multiple sections yielded an age for the reversal of $16.73 \pm 0.13/-0.08$ Ma (95 per cent confidence interval) and identify it as the end of Chron C5Cr of the Gradstein *et al.* (2004) geomagnetic polarity timescale (Jarboe *et al.* 2010).

1.2 Other transitional magnetic field records

Investigations of polarity transitions have revealed several interesting features associated with the reversing field. Directional variation

is usually expressed as virtual geomagnetic poles (VGPs) plotted on maps, which makes comparisons more easy to visualize, and have led recent studies to focus on several questions: (1) do VGPs tend to be confined longitudinally, (2) does the field undergo standstills that result in clustering of VGPs and (3) are there similarities between different reversals (e.g. VGP clusters and longitudinal bands) that might indicate the presence of preferred modes of the reversing field controlled by persistent laterally varying conditions in the lowermost mantle?

Laj *et al.* (1991) showed that four different sedimentary records, spanning 100 ka to at least 10 Ma, yielded transitional VGPs that were confined to one of two longitudinal bands, either across the Americas or Eastern Asia. They speculated that these bands might be caused by long-lived thermal anomalies at the Earth's core-mantle boundary (CMB) imposing patterns of fluid flow in the core. Clement (1991) also found longitudinal banding across the Americas and Eastern Asia in a global compilation of 21 sedimentary records of a single geomagnetic reversal (Matuyama/Brunhes). Because of the inherent smoothing of magnetization variations in sediment records, it has been suggested that these bands might be influenced by or even be entirely artefacts of the recording process (van Hoof & Langereis 1991; Langereis *et al.* 1992). But Hoffman *et al.* (Hoffman 1992; Hoffman *et al.* 2008), relying on the accurate spot readings of the field afforded by volcanic records, proposed that clusters of transitional directions frequently occur when the reversing field stalls for an appreciable length of time, with their VGPs revealing geographically preferred patches. Two of the proposed preferred patches are in the south Atlantic/southern South America and western Australia/eastern Indian Ocean regions. If the preferred patches are real, and not merely clusters due to episodic volcanism, VGP banding seen in sediment records could be a smoothed recording dominated by the average normal and reversed polarity field and a preferred transitional direction. A criticism of the preferred patch hypothesis is that it is based on a restricted set of records and so is susceptible to subjective selectivity; for instance, Prévot & Camps (1993) argued that large compilations of many transitional

VGPs recorded in lavas of age 0–16 Ma is not distinguishable from random distributions.

Love & Mazaud (1997) selected 11 records that passed certain criteria for reliability and temporal resolution from their newer compilation (MBD97) of the numerous records of the most recent, Matuyama/Brunhes reversal. This compilation which includes loess, marine sedimentary and volcanic records, also indicates banding along American and Asian-Australian longitudes. Taking an entirely different approach, Leonhardt & Fabian (2007) used iterative Bayesian inversion on four transition records to create a

paleomagnetic reconstruction of the global geomagnetic field during the Matuyama/Brunhes transition that does a reasonably good job of reproducing many other records of the same reversal. Their synthetic model contains banding of VGPs between 200°E and 250°E, which is in a broad eastern Pacific/western North America band. Love (1998, 2000) considered transitional directions from lava flows spanning the last 20 Ma and claimed a slight statistical significance for preferred VGP bands over the Americas and Asia. Hoffman *et al.* (2008) show that persistent core–surface flux concentrations can exist in some locations for tens of Ma.

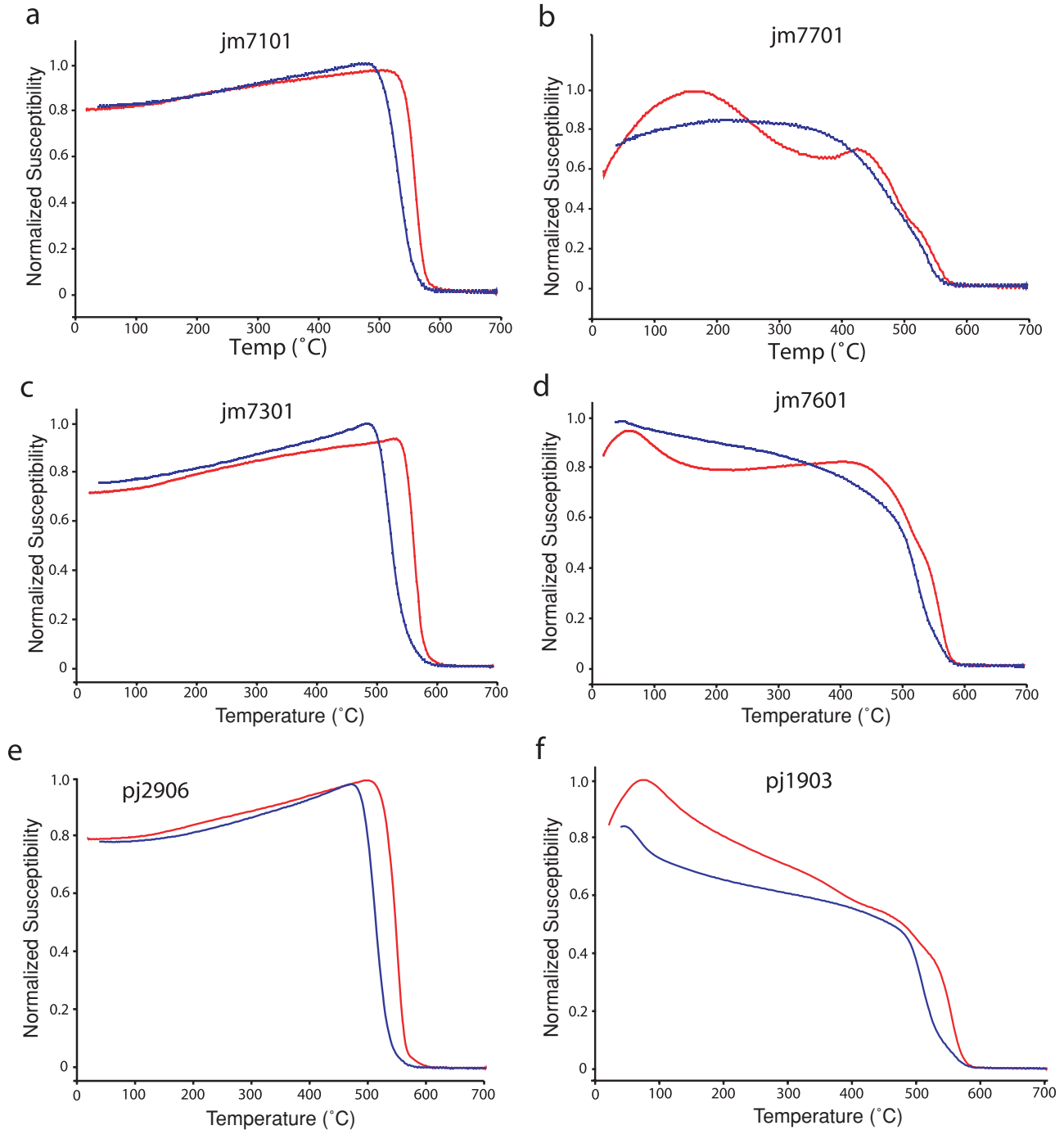


Figure 2. Susceptibility versus temperature curves, run in argon atmosphere. Heating curves in red and cooling curves in blue. Plots a, c and e show samples that appear to be dominated by Ti-poor titanomagnetite. Plots b, d and f illustrate samples that contain an additional magnetic mineral that undergoes alteration upon heating, likely titanomaghemite that alters to magnetite.

In further support of banding, Glen *et al.* (1994, 1999) compiled 14 western North America transitional and excursions records in both volcanic and sedimentary rocks of the last ~16 Ma. However, the bands that they found were notably offset (on average 60° eastward) from those identified in compilations of records from sites distributed globally (Clement 1991; Laj *et al.* 1991; Tric *et al.* 1991). They suggested that this offset reflects the presence of a persistent non-dipole field component of the reversing field.

Numerical modelling of the geodynamo provides independent support for the presence of preferred longitudinal VGP bands. Coe *et al.* (2000) studied the behaviour of the transitional field during two reversals of the Glatzmaier *et al.* (1999) simulation in which the pattern of CMB heat flow was set as a boundary condition as inferred from seismic tomography. During these two reversals, VGPs from sites evenly distributed over the globe showed a peak in density between 260°E and 310°E and low density of VGPs over the much of the Pacific basin. The computationally less demanding simulations of Olson *et al.* (2002) and Kutzner & Christensen (2004), which could be run for long enough to encompass many reversals,

exhibit clearly significant banding related to longitudinal highs in imposed CMB heat flux. A more complex picture, however, was revealed in heuristic simulations (Quidelleur & Valet 1996; Valet & Plenier 2008), which is reminiscent of Cox's (1968) conceptual model for the triggering of reversals. Valet & Plenier (2008) simulated reversals by decreasing the axial dipole field to zero in the 0–7 ka geomagnetic field model CALS7K of Korte & Constable (2005) while leaving the non-dipole field alone. VGPs from equally distributed sites produced a single longitudinal band from about 0° to 60°. By simulating the sediment magnetization process, VGP paths were smoothed resulting in VGPs that were more strongly banded longitudinally. No VGP clustering was displayed in the simulation.

To sum up, after 20 years of research and discussion of the behaviour of VGP paths during reversals, the scientific community has yet to reach a firm consensus on VGP path behaviour and meaning. The bulk of the evidence, however, tends to suggest that, although any one VGP reversal path as seen from a certain position on Earth may behave in a pseudo-random way, the average of a large number of these paths has features that are likely related to the pattern of

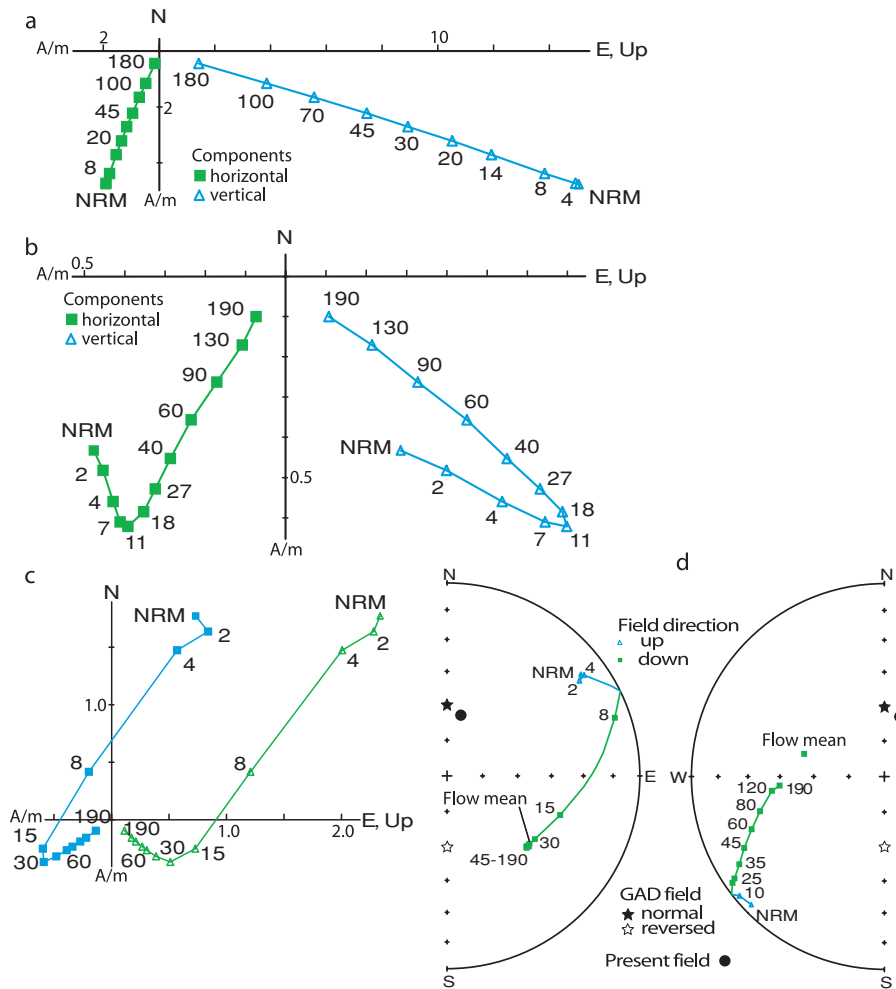


Figure 3. (a) Orthogonal vector component diagram in stratigraphic coordinates of a well-behaved alternating field (AF) demagnetization to 180 mT of reversely magnetized specimen jm0201a from the Poker Jim South-A section. Natural remanent magnetization (NRM) is 15.0 A m⁻¹. (b) Sample pj0506a from the Poker Jim North section with a normal overprint removed by about 18 mT. NRM = 0.7 A m⁻¹. (c) Orthogonal vector component diagram and stereonet plot of the AF demagnetization to 190 mT of specimen cp1204a from the Catlow section. Removal of a probable lightning overprint, indicated by rapid drop in magnetization accompanying large directional change in low alternating fields, is complete by about 45 mT. NRM = 3.3 A m⁻¹. (d) Stereonet plot of the AF demagnetization to 190 mT of specimen cp2204a from the Catlow section. A strong lightning overprint is not completely removed, but the great circle path is directed toward the flow mean direction. NRM = 50.5 A m⁻¹.

heat-flow at the CMB. The composite Steens reversal path, as discussed later in this paper, provides support for this conclusion.

2 PALEOMAGNETIC PROCEDURES

2.1 Sampling

The goal of this study was to improve the existing paleomagnetic record of the Steens reversal (Mankinen *et al.* 1985; Camps *et al.* 1999) by splicing in new directions not found at Steens Mountain that were recorded by lavas at other sections. Other reconnaissance studies on the Oregon Plateau had shown that a reversal at the Catlow (Minor 1986) and Poker Jim South (Goldstein *et al.* 1969) sections was thought to be the same as the Steens Mountain event. We, too, found transitional directions in these sections and also in a previously unstudied section at Poker Jim North (Fig. 1) that proved to record the Steens reversal. We also studied several other localities but found no transitional directions (Jarboe *et al.* 2008).

For this study to be a success, it was critical to sample all of the lava flows in a section that erupted during the polarity transition. It was also important for the sections to be well exposed to reveal a flow-on-flow sequence. The northwestern Great Basin is cut by a series of normal faults with significant throw that expose large sections of sparsely vegetated CRBG lavas (Supporting Information—Photos). A portable flux-gate magnetometer was used in the field to help determine the magnetic polarity of some flows before drilling. If upon analysis in the laboratory and reference to field notes it appeared that useful transitional flows had been skipped, we returned to complete the sampling.

All paleomagnetic procedures and analyses were performed at the University of California, Santa Cruz. Paleomagnetic cores 2.5-cm diameter were cut with a water-cooled, diamond-studded,

hollow core bit driven by a hand-held gasoline powered drill. The cores were usually 5- to 10-cm long and oriented to an accuracy of 1° – 2° while still attached to the outcrop using an orienting stage and a Brunton compass. Sightings of the sun and points of known direction were used to correct for local magnetic anomalies at each drill hole. Flow bottoms were generally drilled to minimize the chance of remagnetization by overlying flows. The orientation angles were recorded to the nearest degree and time to the nearest minute. In the laboratory, the cores were cut into 2.5-cm-long specimens. In general the deepest, least weathered specimens from each core were used when determining the paleomagnetic field directions.

2.2 Rock magnetic properties, demagnetization, and sample directions

Magnetic susceptibility versus temperature for six representative samples heated and cooled in argon are plotted in Fig. 2. The single Curie temperature near 580°C of the heating curves and the nearly reversible heating and cooling cycles of Figs 2(a), (c) and (e) indicate the dominance of magnetite. In addition to magnetite, the heating curves of Figs 2(b), (d) and (f) reveal a magnetic mineral with lower Curie temperature that is mainly absent from the cooling curves. This mineral is probably titanomaghemite that inverts to magnetite plus ilmenite during laboratory heating. The magnetic properties of the Steens Basalt were studied in detail by Mankinen *et al.* (1985) in preparation for paleointensity studies reported by Prevot *et al.* (1985). They measured the saturation magnetization (J_s) and saturation remanence (J_{rs}) for 166 samples. In general J_{rs}/J_s values from their study are indicative of pseudo-single domain grains or a mixture of domain types. They also performed storage tests on 716 samples for viscous magnetization, which gave a low

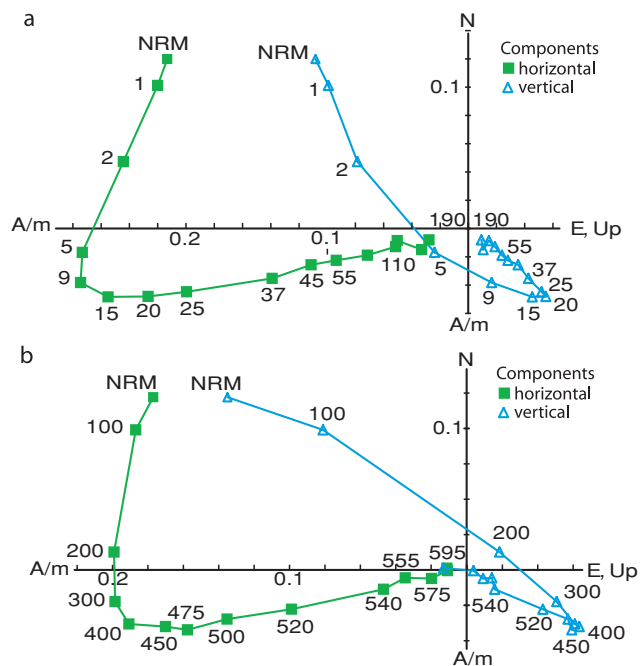


Figure 4. (a) AF demagnetization of specimen jm7401a from the Poker Jim South-B section. Demagnetization steps are in mT. $\text{NRM} = 0.30 \text{ A m}^{-1}$. (b) Thermal demagnetization of a specimen from the same core (specimen jm7401b) with a similar demagnetization path and ChRM direction. Demagnetization steps in $^{\circ}\text{C}$. $\text{NRM} = 0.31 \text{ A m}^{-1}$.

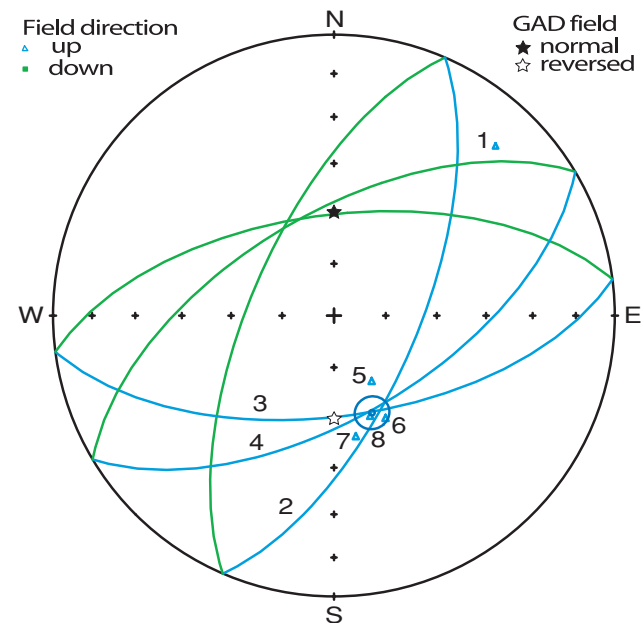


Figure 5. Determining the flow mean direction of flow cp48 ($\alpha_{95} = 4.9^{\circ}$) from the Catlow section. Specimen 1 was overprinted by lightning to such an extent ($\text{NRM} = 228 \text{ A m}^{-1}$) that the ChRM was obliterated. Specimens 2–4 were overprinted with lightning but decayed along great circles toward the cluster of stable directions. Specimens 5–8 yielded stable directions that decayed univectorially to the origin, revealing the ChRM directly. The flow mean direction was determined using the method of McFadden & McElhinny (1995).

Table 1. Paleomagnetic field directions, VGPs and geographic locations of the flows and the directional groups from the Poker Jim South, Poker Jim North and Catlow sections. Flows are listed from oldest to youngest down the table.

DG	Flow ID	N ₀	N	LF	GC	D°	I°	k	α ₉₅	Long°	Lat°	dp	dm	A ₉₅	FNS	°N	°W	el(m)	Rotated to North America			
																			D°	I°	Long°	Lat°
Poker Jim North (PN)																						
1	pj01	8	7	5	2	245.8	-59.3	96	6.4	129.9	-41.9	7.2	9.6	8.3	1	42.70643	119.56562	1488	231.3	-59.3	136.4	-52.0
1	pj02	7	7	4	3	247.3	-57.8	294	3.7	131.2	-40.1	4.0	5.4	4.6	0	42.70630	119.56550	1507	232.8	-57.8	138.1	-50.3
1	pj03	8	8	4	4	246.1	-58.5	63	7.4	130.8	-41.3	8.1	11.0	9.4	0	42.70640	119.56517	1511	231.6	-58.5	137.6	-51.5
2	pj04	8	8	7	1	219.6	-57.0	28	10.8	146.5	-59.6	11.4	15.7	13.4	0	42.70613	119.56525	1523	205.1	-57.0	156.9	-70.2
2	pj05	8	8	7	1	221.0	-52.3	164	4.4	153.6	-56.5	4.1	6.0	5.0	0	42.70582	119.56512	1513	206.5	-52.3	166.8	-67.0
3	pj06	8	8	8	0	199.5	-38.3	648	2.2	196.7	-63.3	1.5	2.6	2.0	0	42.70577	119.56512	1525	185.0	-38.3	227.7	-68.4
3	pj07	8	8	8	0	197.9	-33.3	270	3.4	203.1	-61.2	2.2	3.9	2.9	0	42.70558	119.56523	1525	183.4	-33.3	232.6	-65.3
3	pj08	8	8	8	0	196.3	-31.5	92	5.8	207.0	-60.8	3.6	6.5	4.8	0	42.70547	119.56527	1524	181.8	-31.5	236.4	-64.3
3	pj09	8	8	8	0	200.4	-36.4	369	2.9	196.7	-61.7	2.0	3.4	2.6	0				185.9	-36.4	226.1	-67.0
3	pj10	8	8	8	0	201.3	-34.9	346	3.0	196.3	-60.4	2.0	3.5	2.6	0				186.8	-34.9	224.6	-65.8
3	pj11	8	8	8	0	202.9	-37.9	93	5.8	191.4	-61.3	4.0	6.8	5.2	0	42.70558	119.56535	1550	188.4	-37.9	219.6	-67.4
4	pj12a	5	5	3	2	169.2	-16.0	217	5.6	258.9	-54.2	3.0	5.8	4.2	0				154.7	-16.0	280.5	-48.9
5	pj12b	3	3	3	0	137.5	4.9	190	9.0	292.2	-30.8	4.5	9.0	6.4	0				123.0	4.9	304.9	-21.8
5	pj13	8	7	6	1	138.4	7.7	227	4.1	290.4	-30.2	2.1	4.1	2.9	0	42.70557	119.56545	1551	123.9	7.7	303.1	-21.3
5	pj14	5	5	5	0	134.9	6.8	218	5.2	294.0	-28.5	2.6	5.2	3.7	0	42.70537	119.56513	1561	120.4	6.8	306.2	-19.3
6	pj15	8	8	7	1	139.1	14.2	87	6.0	287.6	-27.8	3.1	6.1	4.3	0				124.6	14.2	300.3	-19.2
7	pj16	8	8	3	5	150.3	41.6	91	6.2	268.8	-18.0	4.6	7.6	5.9	0	42.70545	119.56563	1570	135.8	41.6	281.0	-11.9
7	pj17	8	8	8	0	154.0	37.0	157	4.4	266.7	-22.3	3.0	5.2	3.9	0	42.70510	119.56598	1577	139.5	37.0	279.7	-16.5
7	pj18	8	8	5	3	152.7	36.4	119	5.3	268.1	-22.2	3.6	6.2	4.7	0	42.70503	119.56595	1583	138.2	36.4	281.0	-16.2
7	pj19	8	8	7	1	151.7	41.6	162	4.4	267.6	-18.4	3.3	5.4	4.2	0				137.2	41.6	279.9	-12.6
7	pj20	8	8	8	0	149.7	36.9	400	2.8	270.8	-20.8	1.9	3.3	2.5	0				135.2	36.9	283.3	-14.5
7	pj21	8	7	7	0	153.3	39.5	114	5.7	266.7	-20.4	4.1	6.8	5.3	0				138.8	39.5	279.4	-14.6
8	pj22	8	7	6	1	138.6	50.9	43	9.4	274.9	-6.6	8.6	12.7	10.5	0				124.1	50.9	285.3	0.3
8	pj23	8	8	8	0	148.0	45.5	175	4.2	269.6	-14.4	3.4	5.3	4.2	0				133.5	45.5	281.2	-8.2
8	pj24	8	8	3	5	138.7	45.0	39	9.7	277.4	-11.0	7.8	12.3	9.8	0				124.2	45.0	288.2	-3.8
9	pj25	8	7	5	2	24.3	61.8	65	7.7	321.1	72.2	9.2	11.9	10.5	0				9.8	61.8	324.7	82.8
10	pj26	8	8	8	0	27.0	51.0	228	3.7	348.7	66.0	3.4	5.0	4.1	0	42.70503	119.56565	1594	12.5	51.0	14.3	75.2
11	pj27	8	8	8	0	22.9	58.5	68	6.7	334.1	72.4	7.4	9.9	8.6	0				8.4	58.5	356.4	82.8
12	pj28	8	8	7	1	35.0	80.9	70	6.7	258.7	56.0	12.5	12.9	12.7	0	42.70503	119.56555	1609	20.5	80.9	252.3	58.9
13	pj29	8	8	8	0	29.7	70.1	135	4.8	289.7	67.5	7.1	8.3	7.7	0	42.70483	119.56553	1616	15.2	70.1	276.4	74.8
13	pj30	7	5	5	0	39.3	69.3	254	4.8	295.1	62.1	7.0	8.2	7.6	0	42.70490	119.56562	1622	24.8	69.3	290.0	70.6
13	pj31	8	8	8	0	29.4	64.4	175	4.2	310.7	68.8	5.4	6.7	6.0	0	42.70467	119.56548	1637	14.9	64.4	306.9	78.8
13	pj32	8	8	8	0	29.8	68.7	238	3.6	294.9	68.0	5.2	6.1	5.6	0				15.3	68.7	282.9	76.1
14	pj33	8	8	8	0	25.4	76.3	137	4.8	266.0	64.2	8.2	8.9	8.5	0	42.70450	119.56542	1644	10.9	76.3	253.1	67.8
14	pj34	8	8	7	1	35.2	75.9	272	3.4	272.8	61.1	5.8	6.3	6.0	0	42.70450	119.56548	1650	20.7	75.9	263.5	66.1
14	pj35	8	8	8	0	34.1	72.6	64	7.0	282.9	63.9	11.0	12.4	11.7	0				19.6	72.6	272.6	70.4
15	pj36	8	8	5	3	342.6	74.3	95	5.9	216.0	69.2	9.7	10.7	10.2	0	42.70428	119.56538	1671	328.1	74.3	204.6	63.8
16	pj37	8	8	8	0	339.7	45.9	219	3.8	113.9	67.4	3.1	4.9	3.9	0				325.2	45.9	133.1	57.9
16	pj38	8	8	8	0	345.8	46.0	338	3.0	101.9	70.8	2.5	3.8	3.1	0	42.70397	119.56563	1681	331.3	46.0	126.3	62.2
16	pj39	8	8	8	0	334.9	48.9	157	4.4	125.9	66.2	3.8	5.8	4.7	0	42.70363	119.56590	1682	320.4	48.9	141.4	55.9
17	pj40	7	6	4	2	343.6	62.6	133	6.1	162.1	78.0	7.5	9.5	8.4	n/a	42.70363	119.56590	1691	329.1	62.6	164.3	67.6
Grouped flows																						
1	pj1-3	23	22	13	9	246.3	-58.6	111	3.0	130.6	-41.2	3.3	4.5	3.9				231.8	-58.6	137.3	-51.4	
2	pj4-5	16	16	14	2	220.4	-54.6	48	5.4	150.3	-58.0	5.4	7.6	6.4				205.9	-54.6	162.4	-68.6	
3	pj6-11	48	48	48	0	199.7	-35.4	161	1.6	198.6	-61.5	1.1	1.8	1.4				185.2	-35.4	228.1	-66.4	
5	pj12b-14	16	15	14	1	136.9	6.8	222	2.6	292.1	-29.7	1.3	2.6	1.8				122.4	6.8	304.7	-20.7	
7	pj16-21	48	47	38	9	152.1	38.6	145	1.7	268.1	-20.6	1.2	2.0	1.5				137.6	38.6	280.7	-14.6	
8	pj22-24	24	23	17	6	142.0	47.3	58	4.0	273.8	-10.7	3.4	5.2	4.2				127.5	47.3	284.8	-4.0	
13	pj29-32	31	29	28	1	31.2	68.0	167	2.1	297.9	67.3	3.0	3.5	3.2				16.7	68.0	288.3	75.9	
14	pj33-35	24	24	23	1	31.8	75.0	113	2.8	273.9	63.2	4.7	5.1	4.9				17.3	75.0	262.7	68.3	
16	pj37-39	24	24	24	0	340.2	47.0	167	2.3	114.6	68.4	1.9	3.0	2.4				325.7	47.0	134.0	58.8	
Poker Jim South (PS)																						
1	jm01	8	7	7	0	191.2	-59.6	400	3.0	161.1	-81.3	3.4	4.5	3.9	11	42.63923	119.63642	1462	176.7	-59.6	290.3	-86.7
1	jm02	8	8	8	0	184.8	-63.6	161	4.4	111.7	-85.7	5.5	7.0	6.2	7	42.63880	119.63622	1493	170.3	-63.6	354.2	-82.5
1	jm03	8	7	7	0	176.4	-62.2	757	2.2	350.1	-87.2	2.7	3.4	3.0	6	42.63871	119.63590	1516	161.9	-62.2	340.4	-76.8
1	jm04	8	8	8	0	184.1	-56.5	326	3.1	209.4	-83.6	3.2	4.5	3.8	4	42.63868	119.63554	1559	169.6	-56.5	299.1	-80.3
1	jm05	10	10	10	0	181.0	-57.4	321	2.7	230.6	-85.4	2.9	3.9	3.4	0	42.63865	119.63500	1593	166.5	-57.4	310.9	-78.7
2	jm06	8	8	8	0	171.8	-54.5	127	4.9	283.2	-80.1	4.9	6.9	5.8	1				157.3	-54.5	314.7	-70.8
3	jm07	8	8	8	0	133.1	-59.8	191	4.0	343.5	-55.3	4.5	6.0	5.2	11				118.6	-59.8	349.8	-45.1
4	jm08	8	8	8	0	146.9	-61.2	644	2.2	341.0	-65.7	2.6	3.4	3.0	5	42.63898	119.63379	1656	132.4	-61.2	346.5	-55.3
5	jm09	8	8	8	0	145.0	-68.4	244	3.6	3.6	-64.8	5.1	6.1	5.6	0				130.5	-68.4	3.2	-55.8
6	jm10	8	8	8	0	179.7	-49.3	171	4.3	241.6	-77.6	3.8	5.7	4.7	5				165.2	-49.3	288.8	-72.8
6	jm11	8	8	8	0	181.0	-53.7	422	2.7	234.7	-81.6	2.6	3.8	3.1	4	42.63899	119.63331	1752	166.5	-53.7	296.5	-76.5
7	jm12	8	8	8	0	195.1	-61.1	171	4.2	147.5	-78.9	4.9	6.4	5.6	n/a				180.6	-61.1	194.4	-89.4
6	jm49	6	6	6	0	182.9	-53.7	692	2.5	224.3	-81.3	2.4	3.5	2.9	0	42.62347	119.63					

Table 1. (Continued.)

DG	Flow ID	N_0	N	LF	GC	D°	I°	k	α_{95}	Long $^\circ$	Lat $^\circ$	dp	dm	A_{95}	FNS	$^\circ N$	$^\circ W$	el(m)	Rotated to North America			
																			D°	I°	Long $^\circ$	Lat $^\circ$
6	jm53	8	8	8	0	182.4	-54.8	237	3.6	225.2	-82.5	3.6	5.1	4.3	0			167.9	-54.8	296.6	-78.1	
7	jm54	6	6	6	0	188.6	-60.3	314	3.8	159.5	-83.5	4.4	5.8	5.1	0			174.1	-60.3	315.1	-85.4	
8	jm55	9	9	9	0	176.3	-61.3	568	2.2	327.6	-87.3	2.6	3.4	3.0	0	42.62330	119.63865	1767	161.8	-61.3	335.7	-76.6
9	jm56	8	8	8	0	189.4	-64.3	154	4.5	119.7	-82.4	5.8	7.2	6.5	0	42.62357	119.63847	1772	174.9	-64.3	15.9	-85.0
9	jm57	8	8	8	0	203.1	-65.7	127	4.9	124.3	-73.0	6.5	8.0	7.2	0			1773	188.6	-65.7	106.1	-82.0
10	jm58	8	8	8	0	225.5	-58.6	159	4.4	140.2	-55.9	4.9	6.5	5.6	0	42.62358	119.63500	1775	211.0	-58.6	147.9	-66.5
10	jm59	8	8	8	0	220.5	-57.4	551	2.4	145.1	-59.1	2.6	3.5	3.0	0	42.62287	119.63833	1780	206.0	-57.4	154.7	-69.7
10	jm60	8	8	8	0	219.9	-58.7	509	2.5	142.8	-60.0	2.8	3.7	3.2	0	42.62280	119.68300	1780	205.4	-58.7	151.2	-70.7
10	jm61	8	8	8	0	223.5	-56.1	445	2.6	145.7	-56.3	2.7	3.7	3.2	0			209.0	-56.1	155.6	-67.0	
10	jm62	8	8	8	0	222.8	-51.3	101	5.5	153.5	-54.7	5.1	7.5	6.2	0	42.62256	119.63835	1803	208.3	-51.3	166.5	-65.3
10	jm63	8	8	8	0	221.0	-53.0	235	3.6	152.4	-56.8	3.5	5.0	4.2	0			206.5	-53.0	165.1	-67.4	
10	jm64	8	8	8	0	218.3	-55.0	242	3.6	150.9	-59.7	3.6	5.1	4.3	0	42.62238	119.63834	1812	203.8	-55.0	163.5	-70.3
10	jm65	8	7	6	1	221.0	-54.5	251	3.9	149.9	-57.5	3.9	5.5	4.6	0	42.62234	119.63824	1812	206.5	-54.5	161.8	-68.1
10	jm66	8	6	6	0	220.3	-52.9	317	3.8	153.0	-57.3	3.6	5.3	4.4	0	42.62265	119.63812	1814	205.8	-52.9	166.2	-67.8
10	jm67	8	8	8	0	220.2	-54.2	55.8	7.5	151.0	-58.0	7.4	10.5	8.8	0	42.62240	119.63815		205.7	-54.2	163.3	-68.6
10	jm68	8	8	7	1	220.1	-58.9	23.7	11.7	142.2	-59.9	3.0	17.4	7.2	0	42.62241	119.63802	1805	205.6	-58.9	150.5	-70.6
10	jm69	8	7	7	0	229.4	-54.0	617	2.4	145.4	-51.1	2.4	3.4	2.9	0	42.62243	119.63794	1822	214.9	-54.0	155.3	-61.8
10	jm70	8	8	8	0	231.9	-53.1	137	4.7	145.1	-48.9	4.5	6.5	5.4	0	42.62022	119.63925		217.4	-53.1	154.9	-59.5
10	jm71	8	8	6	2	228.1	-54.3	160	4.8	145.8	-52.2	4.7	6.8	5.7	0			213.6	-54.3	155.7	-62.9	
11	jm72	8	8	7	1	2.0	65.3	202	3.9	256.2	85.0	5.1	6.3	5.7	0	42.61972	119.63889	1851	347.5	65.3	183.2	80.0
12	jm73	8	5	3	2	253.0	-25.9	122	7.5	151.5	-21.6	4.4	8.1	6.0	0	42.61893	119.63932	1863	238.5	-25.9	162.0	-32.2
12	jm74	8	8	5	3	253.5	-20.9	210	4.1	153.5	-19.4	2.3	4.3	3.1	0			239.0	-20.9	164.0	-30.0	
13	jm75	8	8	4	4	258.5	-19.0	393	2.9	150.9	-15.0	1.6	3.0	2.2	0	42.61885	119.63927	1867	244.0	-19.0	161.1	-25.6
14	jm76	8	7	2	5	249.1	-28.5	84.8	7.3	153.0	-25.5	4.4	8.0	5.9	0	42.61860	119.63910	1894	234.6	-28.5	163.7	-36.1
15	jm77	8	8	6	2	354.6	64.5	309	3.2	196.5	84.6	4.1	5.1	4.6	0	42.61951	119.63863	1891	340.1	64.5	172.1	75.4
16	jm78	8	8	8	0	349.2	57.3	110	5.3	124.4	80.5	5.7	7.7	6.6	0			334.7	57.3	145.2	70.2	
16	jm79	8	8	7	1	343.4	57.9	529	2.4	138.2	76.8	2.6	3.5	3.0	0	42.61706	119.63759	1871	328.9	57.9	151.2	66.2
16	jm80	8	8	8	0	346.7	57.5	351	3.0	131.0	78.9	3.2	4.4	3.8	0	42.61672	119.63763	1932	332.2	57.5	147.8	68.5
Grouped flows																						
1	jm1-5	40	38	38	0	183.4	-60	202	1.6	188.1	-86.7	1.8	2.4	2.1				168.9	-59.7	320.3	-81.5	
6	jm10-11 jm49-53	55	55	55	0	181.3	-52	208	1.3	233.9	-80.2	1.2	1.8	1.5				166.8	-52.3	291.7	-75.8	
7	jm12 jm54	14	14	14	0	192.3	-61	209	2.8	151.2	-80.9	3.3	4.3	3.8				177.8	-60.8	305.5	-88.2	
9	jm56-57	16	16	16	0	196.1	-65	123	3.3	123.2	-77.8	4.3	5.3	4.8				181.6	-65.1	73.9	-85.3	
10	jm58-71	121	117	109	8	222.9	-55	118	1.2	147.7	-56.4	1.2	1.7	1.4				208.4	-55.1	158.5	-67.0	
12	jm73-74	16	13	6	7	253.0	-23	161	3.4	152.8	-20.7	1.9	3.6	2.6				238.5	-23.3	163.3	-31.2	
16	jm78-80	24	24	23	1	346.6	57.6	222	2.0	131.7	78.9	2.1	2.9	2.5				332.1	57.6	148.2	68.4	
Catlow (C)																						
1	cp65	6	6	6	0	234.8	-61.6	762	2.4	131.4	-50.2	2.9	3.7	3.3	0	42.02707	118.33720	1947	220.3	-61.6	136.4	-60.5
2	cp64	8	8	8	0	234.5	-46.3	32	9.9	151.7	-43.8	8.1	12.7	10.1	2	42.02685	118.33690	1936	220.0	-46.3	162.6	-54.5
3	cp63	8	7	7	0	238.5	-60.3	822	2.1	132.2	-47.1	2.4	3.2	2.8	1	42.02667	118.33688	1941	224.0	-60.3	137.9	-57.5
3	cp62	8	7	7	0	239.0	-57.4	287	3.6	136.3	-45.5	3.8	5.3	4.5	3	42.02685	118.33665	1938	224.5	-57.4	143.3	-56.1
4	cp61	8	7	7	0	226.2	-52.0	998	1.9	150.7	-52.6	1.8	2.6	2.2	3	42.02658	118.33628	1989	211.7	-52.0	161.8	-63.3
5	cp60	7	7	7	0	215.9	-60.6	818	2.1	140.4	-63.4	2.4	3.2	2.8	4	42.02627	118.33590	1997	201.4	-60.6	146.0	-74.1
6	cp58	8	8	5	3	161.5	-68.1	369	3.0	14.1	-74.4	4.2	5.0	4.6	0	42.02638	118.33540	2015	147.0	-68.1	5.4	-65.8
6	cp57	8	7	7	0	150.0	-66.6	540	2.6	0.9	-68.0	3.5	4.3	3.9	0	42.02640	118.33528	2024	135.5	-66.6	0.3	-58.5
6	cp56	8	8	8	0	167.7	-69.2	734	2.0	28.4	-76.4	2.9	3.4	3.1	0	42.02643	118.33462	2033	153.2	-69.2	11.9	-69.1
7	cp55	8	8	8	0	215.0	-66.0	174	4.2	125.2	-64.8	5.6	6.9	6.2	0	42.02608	118.33435	2044	200.5	-66.0	121.0	-74.3
8	cp54	8	8	8	0	202.8	-57.7	387	2.8	156.0	-72.3	3.0	4.1	3.5	0	42.02612	118.33398	2046	188.3	-57.7	179.0	-82.7
9	cp53	8	8	8	0	194.0	-48.1	113	5.2	195.9	-72.9	4.4	6.8	5.5	1	42.02655	118.33382	2045	179.5	-48.1	243.7	-77.1
9	cp52	8	7	6	1	190.8	-55.8	59	8.0	182.2	-79.9	8.2	11.5	9.7	0	42.02642	118.33345	2049	176.3	-55.8	269.8	-83.7
9	cp51	8	8	5	3	193.8	-55.2	277	3.4	177.5	-77.6	3.4	4.8	4.0	0	42.02638	118.33323	2080	179.3	-55.2	246.9	-83.7
10	cp50	8	8	8	0	200.9	-58.3	236	3.6	155.5	-73.9	3.9	5.3	4.5	0	42.02657	118.33315	2074	186.4	-58.3	181.3	-84.3
11	cp49	5	4	4	0	162.5	-70.5	41	14.5	25.5	-72.9	21.7	25.1	23.3	0	42.02782	118.33257	2078	148.0	-70.5	14.0	-65.5
11	cp48	8	7	4	3	158.6	-59.5	169	4.9	332.9	-73.8	5.5	7.4	6.4	0	42.02680	118.33237	2084	144.1	-59.5	340.3	-63.1
12	cp47	7	6	6	0	218.7	-66.2	182	5.0	124.6	-62.3	6.7	8.2	7.4	0	42.02678	118.33162	2108	204.2	-66.2	122.2	-71.8
12	cp46	8	8	8	0	218.8	-64.6	95	5.7	129.1	-62.1	7.3	9.2	8.2	0	42.02692	118.33128	2115	204.3	-64.6	128.9	-72.1
12	cp45	8	8	7	1	220.1	-58.7	51	7.9	142.9	-59.8	8.7	11.7	10.1	0	42.02737	118.33155	2114	205.6	-58.7	150.7	-70.5
13	cp44	8	8	8	0	227.6	-43.3	117	5.1	159.5	-47.6	3.9	6.3	5.0	0	42.02720	118.33095	2115	213.1	-43.3	172.8	-58.0
14	cp43	8	7	7	0	200.8	-42.2	271	3.7	190.8	-65.4	2.8	4.5	3.5	0	42.02742	118.33107	2122	186.3	-42.2	223.2	-71.6
15	cp42	8	8	8	0	101.1	46.5	76	6.4	303.8	10.7	5.3	8.2	6.6	0	42.02750	118.33057	2128	86.6	46.5	312.3	20.5
15	cp41	8	8	7	1	105.0	55.7	145	4.7	295.1	13.9	4.8	6.7	5.7	0	42.02763	118.33062	2140	90.5	55.7	302.9	23.0
15	cp40	8	5	3	2	103.3	50.1	181	6.1	300.1	11.3	5.5	8.2	6.7	1	42.02763	118.33030	2146	88.8	50.1	308.4	20.9
15	cp39	8	8	8	0	103.6	53.2	396	2.8	297.8	13.1	2.7	3.9	3.2	0	42.02802	118.33032	2145	89.1	53.2	305.8	

Table 1. (Continued.)

DG	Flow ID	N_0	N	LF	GC	D°	I°	k	α_{95}	Long $^\circ$	Lat $^\circ$	dp	dm	A_{95}	FNS	$^\circ N$	$^\circ W$	el(m)	Rotated to North America			
																			D°	I°	Long $^\circ$	Lat $^\circ$
19	cp31	9	8	6	2	299.4	32.4	42	8.8	145.6	33.4	5.6	9.9	7.4	1	42.02852	118.32952	2144	284.9	32.4	155.5	22.6
20	cp30	8	8	5	3	296.9	38.5	330	3.2	151.2	34.0	2.3	3.8	3.0	0	42.02892	118.32935	2163	282.4	38.5	160.5	23.3
20	cp29	8	8	6	2	298.2	38.3	58	7.4	150.2	34.9	5.2	8.8	6.8	0	42.02882	118.32913	2174	283.7	38.3	159.6	24.2
21	cp28	8	7	4	3	298.4	46.5	27	12.4	156.5	38.7	10.2	15.9	12.7	1	42.02898	118.32903	2189	283.9	46.5	165.1	28.0
22	cp27	8	8	8	0	308.8	47.1	172	4.2	150.3	46.6	3.5	5.4	4.3	0	42.02885	118.32887	2183	294.3	47.1	159.5	35.9
23	cp26	8	8	6	2	298.8	42.2	97	5.8	152.7	37.0	4.4	7.1	5.6	0	42.02903	118.32888	2181	284.3	42.2	161.7	26.3
23	cp25	9	8	4	4	304.1	36.9	20	13.1	145.1	38.7	9.0	15.3	11.7	0	42.02922	118.32867	2178	289.6	36.9	155.0	27.9
23	cp24	8	8	8	0	296.7	44.8	135	4.8	156.1	36.6	3.8	6.1	4.8	0	42.02922	118.32873	2172	282.2	44.8	164.8	26.0
24	cp23	9	7	3	4	284.5	48.1	278	4.0	166.0	29.2	3.4	5.2	4.2	0	42.02925	118.32870	2191	270.0	48.1	174.2	19.0
25	cp22	9	9	4	5	288.2	56.0	26	10.7	171.5	35.8	11.0	15.4	13.0	0	42.02927	118.32847	2191	273.7	56.0	178.7	25.9
26	cp21	8	8	8	0	289.0	62.5	815	1.9	179.4	39.6	2.3	3.0	2.6	2	42.02987	118.32840	2196	274.5	62.5	185.3	30.4
27	cp20	8	8	8	0	293.5	59.6	140	4.7	173.5	41.3	5.3	7.1	6.1	0	42.02987	118.32838	2199	279.0	59.6	179.9	31.5
28	cp19	8	7	7	0	285.5	0.8	101	6.1	141.5	11.7	3.1	6.1	4.3	0	42.03010	118.32813	2197	271.0	0.8	151.3	1.0
29	cp18	8	8	8	0	13.8	39.0	522	2.4	27.3	66.9	1.7	2.9	2.2	0	42.03040	118.32808	2213	359.3	39.0	63.6	70.0
29	cp17	8	8	8	0	12.8	35.6	602	2.3	31.9	65.2	1.5	2.7	2.0	0	42.03002	118.32808	2208	358.3	35.6	65.9	67.6
29	cp16	8	7	7	0	14.3	38.2	347	3.2	26.9	66.2	2.2	3.8	2.9	0	42.03040	118.32813	2221	359.8	38.2	62.2	69.5
30	cp15b	12	12	9	3	10.9	32.2	285	2.6	37.6	63.8	1.7	2.9	2.2	0				356.4	32.2	69.9	65.3
30	cp15	8	7	7	0	11.1	34.8	149	5.0	35.9	65.3	3.3	5.8	4.4	0	42.03062	118.32797	2205	356.6	34.8	69.9	67.0
31	cp14a	8	8	4	4	349.7	-62.9	45	8.7	69.1	3.2	10.7	13.7	12.1	0				335.2	-62.9	79.2	0.9
31	cp14z	8	8	1	7	337.9	-71.8	23	13.2	73.8	-10.4	20.4	23.2	21.8	0	42.03057	118.32798	2213	323.4	-71.8	81.4	-13.4
31	cp14	8	5	3	2	348.2	-66.5	37	13.6	69.4	-1.6	18.4	22.4	20.3	0	42.03023	118.32767	2224	333.7	-66.5	78.6	-3.9
32	cp13a	8	6	3	3	117.6	-65.1	152	5.8	0.7	-46.4	7.6	9.4	8.5	0				103.1	-65.1	5.4	-37.2
33	cp13	8	7	5	2	115.7	51.2	72	7.3	291.8	4.6	6.7	9.9	8.1	0				101.2	51.2	300.6	13.3
34	cp12	8	8	7	1	126.6	45.3	143	4.7	287.7	-5.4	3.8	6.0	4.8	0	42.03068	118.32733	2249	112.1	45.3	297.6	3.0
35	cp11	8	8	4	4	122.6	47.8	40	9.3	289.3	-1.6	7.9	12.1	9.8	0				108.1	47.8	298.7	6.9
36	cp10	8	8	1	7	37.7	22.5	20	14.3	3.3	45.4	8.0	15.2	11.0	0	42.03087	118.32713	2253	23.2	22.5	21.2	53.6
37	cp09	7	6	3	3	354.3	52.8	493	3.2	91.1	80.3	3.1	4.4	3.7	0	42.03108	118.32720	2241	339.8	52.8	129.9	71.9
38	cp05	8	8	4	4	5.7	64.8	43	8.9	280.4	83.8	11.5	14.3	12.8	0	42.03395	118.32943	2265	351.2	64.8	191.7	82.1
39	cp04	8	7	1	6	27.7	52.3	67	8.5	345.2	66.3	8.0	11.7	9.7	0	42.03402	118.32688	2286	13.2	52.3	8.5	76.2
40	cp03	9	8	6	2	25.3	20.8	39	9.1	19.0	51.7	5.0	9.6	6.9	1	42.03298	118.32555	2295	10.8	20.8	41.7	57.4
41	cp02	8	7	4	3	13.5	43.7	121	5.8	23.4	70.1	4.5	7.2	5.7	0	42.03363	118.32413	2317	359.0	43.7	64.9	73.5
41	cp01	8	8	4	4	14.5	47.4	115	5.4	15.9	72.1	4.5	7.0	5.6	n/a	42.03035	118.31887	2339	0.0	47.4	61.7	76.5
Grouped flows																						
3	cp63-62	16	14	14	0	238.8	-58.9	394	2.0	134.2	-46.3	2.2	3.0	2.6					224.3	-58.9	140.6	-56.8
6	cp58-56	24	23	20	3	159.7	-68.2	316	1.7	12.7	-73.3	2.4	2.9	2.6					145.2	-68.2	5.3	-64.7
9	cp53-51	24	23	19	4	193.3	-52.7	92	3.2	187.1	-76.4	3.0	4.4	3.6					178.8	-52.7	248.3	-81.2
11	cp49-48	13	11	8	3	159.5	-63.7	58	6.1	351.4	-74.8	7.7	9.7	8.6					145.0	-63.7	351.3	-64.7
12	cp47-45	23	22	21	1	219.5	-63.0	78	3.5	133.2	-61.4	4.3	5.5	4.9					205.0	-63.0	135.5	-71.7
15	cp42-36	56	53	46	7	101.7	51.5	145	1.6	300.1	13.2	1.5	2.2	1.8					87.2	51.5	308.2	22.8
16	cp35-34	16	15	12	3	54.1	51.7	94	4.0	326.2	46.6	3.7	5.5	4.5					39.6	51.7	335.7	57.3
20	cp30-29	16	16	11	5	297.6	38.4	104	3.7	150.7	34.5	2.6	4.4	3.4					283.1	38.4	160.0	23.8
23	cp26-24	25	24	18	6	299.8	41.6	49	4.3	151.5	37.5	3.2	5.3	4.1					285.3	41.6	160.7	26.8
29	cp18-16	24	23	23	0	13.6	37.5	433	1.5	28.9	66.1	1.0	1.8	1.3					359.1	37.5	64.0	69.0
30	cp15-15b	20	19	16	3	11.0	33.2	212	2.3	36.9	64.3	1.5	2.6	2.0					356.5	33.2	69.9	65.9
31	cp14a-14	24	21	8	13	345.4	-66.5	36	5.4	71.2	-1.9	7.3	8.9	8.1					330.9	-66.5	80.4	-4.5
41	cp2-1	16	15	8	7	14.1	45.6	120	3.6	19.6	71.1	2.9	4.6	3.7					359.6	45.6	63.1	75.0

Flow mean directions were calculated using PMGSC4.2 (Enkin 2005). VGPs calculated using PaleoMac (Cogne 2003). Sections are flat lying except for Catlow where the data were corrected for strike 335°, dip 12° E. DG, identification number for each group of directions; Flow ID, label given the flow in the field; N_0 , number of cores measured from the flow; N , number of specimens used to determine mean flow direction; LF (GC), number of specimens with magnetic directions determined by a line-fit to the origin (great circle fits), D (I), mean magnetic declination (inclination) of the flow; k , precision parameter of the mean direction; α_{95} , 95 per cent confidence limit on the mean direction; Long (Lat), longitude (latitude) of the virtual geomagnetic pole (VGP); A_{95} , 95 per cent confidence limit on the VGP; FNS, number of flows not sampled between the flow and the next higher one; el, elevation of the flow from handheld GPS and n/a, not available or not applicable.

geometric mean viscosity index of 3.3 ± 0.3 per cent. In general, the magnetic properties of the Steens basalts are straightforward and suggest that they should preserve a reliable characteristic remanent magnetization (ChRM).

The specimens were stepwise-demagnetized, using an average of 11 steps, in a decaying alternating field (AF) of up to 200 mT. Twelve-position measurements of remanent magnetization were measured in a 2G Enterprises superconducting magnetometer equipped with custom built hardware and software described in detail by Morris *et al.* (2009). An Agico JR-5 calibration sample was measured at least daily and kept within 1.2° of the expected direction with an estimated error no greater than 1.2°. For most specimens the ChRM was determined with straight-line fits anchored to the origin (Kirschvink 1980) for the directions that define

the highest stability component in vector component plots. For the rest, great circles were calculated (McFadden & McElhinny 1988) using the software of Enkin (2005). Most specimens showed little secondary magnetization (Fig. 3a). Any viscous overprint was typically removed by AF demagnetization at 2–20 mT (Fig. 3b). A few specimens, often with high initial magnetic intensities compared to others in the same flow, required greater demagnetization fields to reveal the ChRM, but in most cases a well-defined direction was determined (Fig. 3c). We interpret these secondary components to be isothermal remanent magnetization (IRM) produced by strong magnetic fields due to lightning strikes. In areas of unusually strong apparent lightning remagnetization, some specimens had overprints that were not entirely removed even at the highest (~200 mT) demagnetization steps (Fig. 3d). In such cases, the magnetic direction

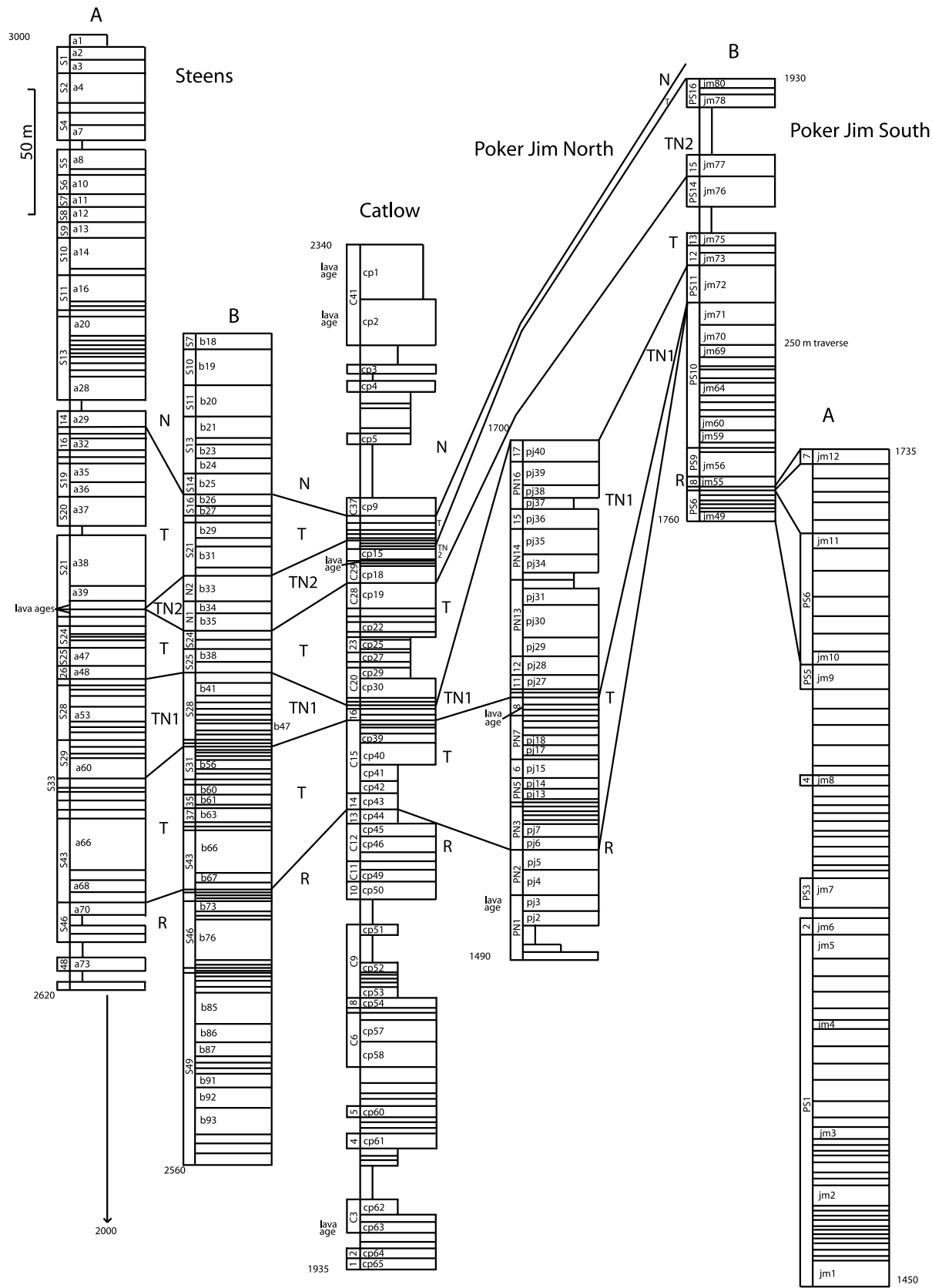


Figure 6. Stratigraphic columns for the Steens A and B, Catlow, Poker Jim North and Poker Jim South A and B sections. Elevations are in metres. R, N, T (reversed, normal, transitional flows). TN1 are flows erupted during the first transitional normal and TN2 are flows erupted during the second transitional normal. Vertical labels on the left of the columns indicate directional groups. Horizontal labels inside flows are flow IDs.

Poker Jim North

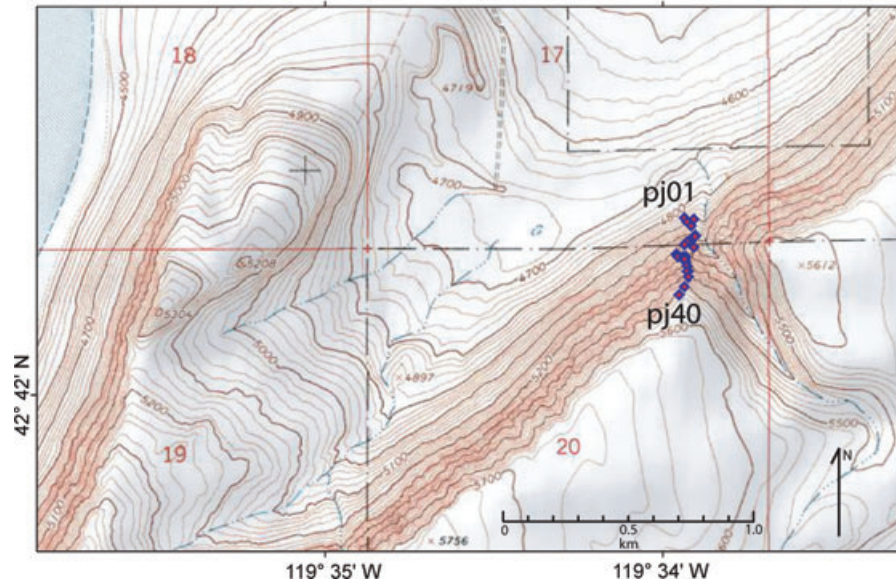


Figure 7. Flow locations for the Poker Jim North section.

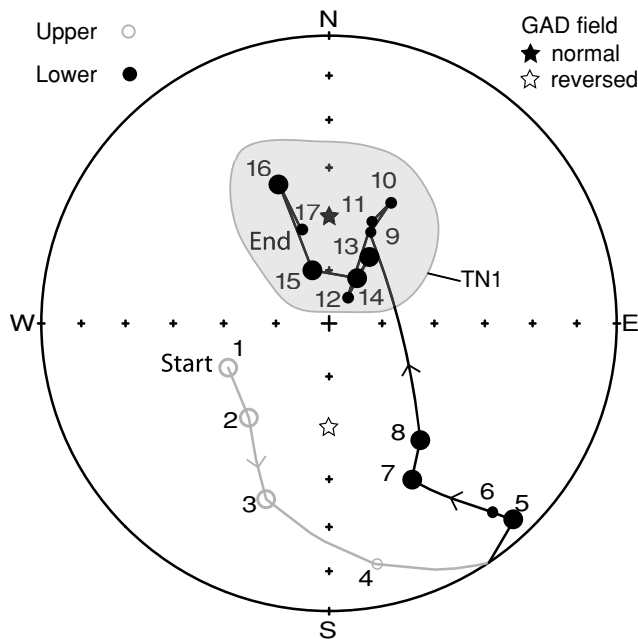


Figure 8. Paleomagnetic directional groups for the Poker Jim North Section. Smaller symbols indicate groups containing only one flow. TN1 are directional groups found in the first transitional normal. In this and all later figures showing directional data the α_{95} circles have been omitted for clarity. They may be found in Table 1.

during AF demagnetization usually followed a great circle path towards the ChRM direction determined from other samples in the same flow.

A few samples were thermally demagnetized to compare the results with those for sister specimens that were treated with AF demagnetization. In general, the thermal demagnetization directions agree with the AF demagnetization results. For core jm7401, which has a relatively large normal overprint, both AF and thermal demagnetization methods yielded a similar ChRM direction of

$D = 256.7, I = -17.2, \alpha_{95} = 1.5$ for the AF demagnetization and $D = 258.4, I = -21.0, \alpha_{95} = 1.5$ for the thermal demagnetization (Fig. 4). This similarity between thermal and AF demagnetization directions gives us confidence that the ChRMs from our AF demagnetization experiments accurately represent the directions of the paleomagnetic field. Note the unusual Curie temperature (400°C) of the secondary component. This behaviour has been seen in other Steens Basalt samples (Camps *et al.* 1995) and was attributed to the mineral magnesioferrite.

2.3 Flow mean directions

In almost all cases, at least eight samples were taken from each flow, and the flow mean directions and confidence limits (Fisher 1953) were calculated using the ChRM directions determined from straight-line fits to demagnetization points that decayed to the origin, as in Fig. 3(a) and (b). When the ChRM of one or more samples was not isolated by demagnetization but instead displayed directions that moved progressively along a great circle, as in Fig. 3d, McFadden & McElhinny (1995) statistics were used. For an example of a case requiring this type of analysis, see Fig. 5. Paleomagnetic data, including VGPs, locations and elevations of the flows are shown in Table 1. Directions were rejected when samples had lightning overprints (L) so strong as to completely overwhelm the ChRM, had unstable demagnetization paths (U), or had resolvable characteristic directions but with outlying directions greater than 40° from the flow mean direction (O). At the Poker Jim North section, 314 cores were measured: 267 gave resolvable characteristic directions, 39 yielded great circle fits and 8 directions were rejected (3 L, 1 U, 4 O). At the Poker Jim South section, 351 cores were measured with 319 giving resolvable characteristic directions, 22 yielding great circle fits and 10 were rejected (4 L, 1 U, 5 O). At the Catlow section, 521 cores were measured with 383 giving resolvable characteristic directions, 105 yielding great circle fits and 33 were rejected (24 L, 1 U, 8 O). Specimens completely overprinted by lightning tend to have shallow directions, much stronger NRM than other specimens in the flow, directions far from the flow mean, and no low-stability

direction consistent with a viscous component acquired in a geocentric axial dipole (GAD) field (see Fig. 5, specimen 1, for an example).

2.4 Directional groups

As is often the case when sampling high-resolution volcanic sections, back-to-back flows may show little difference in their paleomagnetic directions, presumably because they erupted in relatively rapid succession. When this is the case, a more representative sampling of geomagnetic field variation is generally obtained by grouping successive flows with the same or similar directions into the

equivalent of a single thick flow. We use the method described by Mankinen *et al.* (1985) to group flow packets of superposed lavas at Steens Mountain and used by Jarboe *et al.* (2008) on full-polarity, Steens-equivalent sections. Sequential lava flow mean directions whose α_{95} values overlap are combined unless they trend in a consistent direction, in which case they are not grouped. A schematic stratigraphic column with flows and their directional groups are given in Fig. 6.

3 VOLCANIC SECTIONS

3.1 Poker Jim North

The Poker Jim North section (42.70°N, 119.57°W) is located 82 km west of Steens Mountain at the north end of Poker Jim Ridge (Fig. 7). It lies 2 km to the east of the main Poker Jim Ridge escarpment with a possible fault lying in-between. Every one of the 40 flows exposed at the 200 m section was sampled and the resultant magnetization directions were combined into 17 flow groups. The flow mean directions are well behaved with only one flow having an α_{95} greater than 10°. All of the flow groups have an α_{95} less than

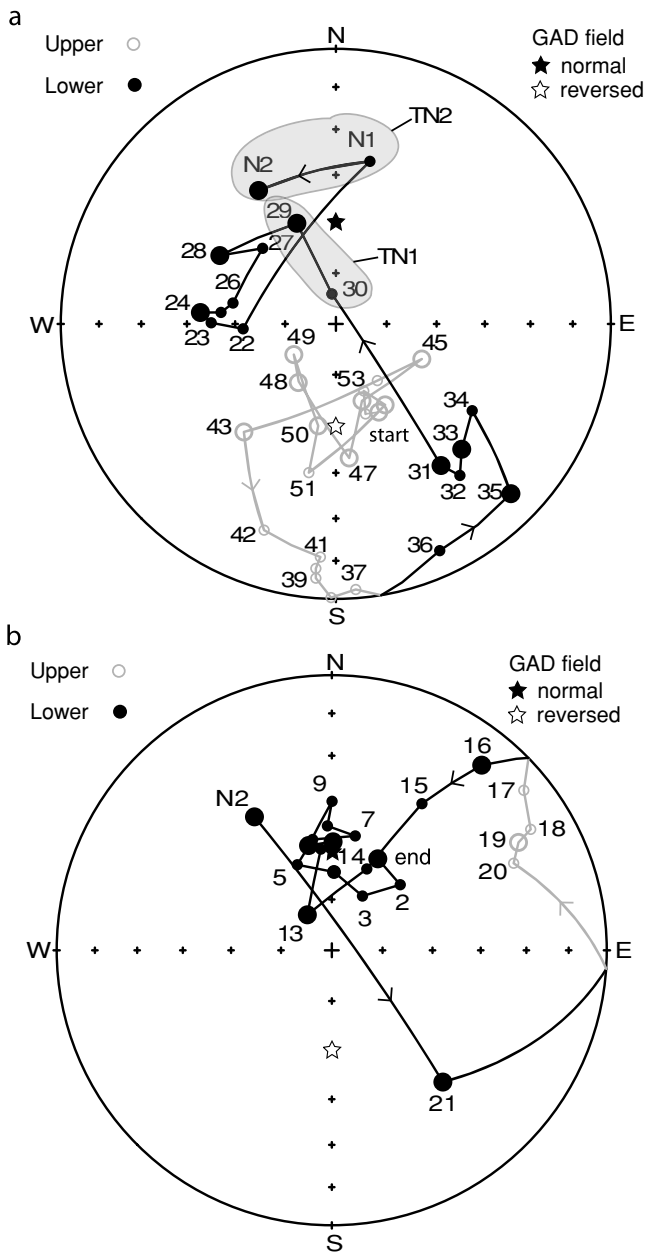


Figure 9. Magnetic field directions of flow groups found at Steens Mountain. Figure (b) is a continuation of the path from (a). Numbers are flow groups from Mankinen *et al.* (1985). Groups N1 and N2 are additional groups found at Steens Mountain by Camps *et al.* (1999). Smaller symbols indicate groups consisting of a single flow. TN1 and TN2 are the first and second transitional normal groups, respectively.

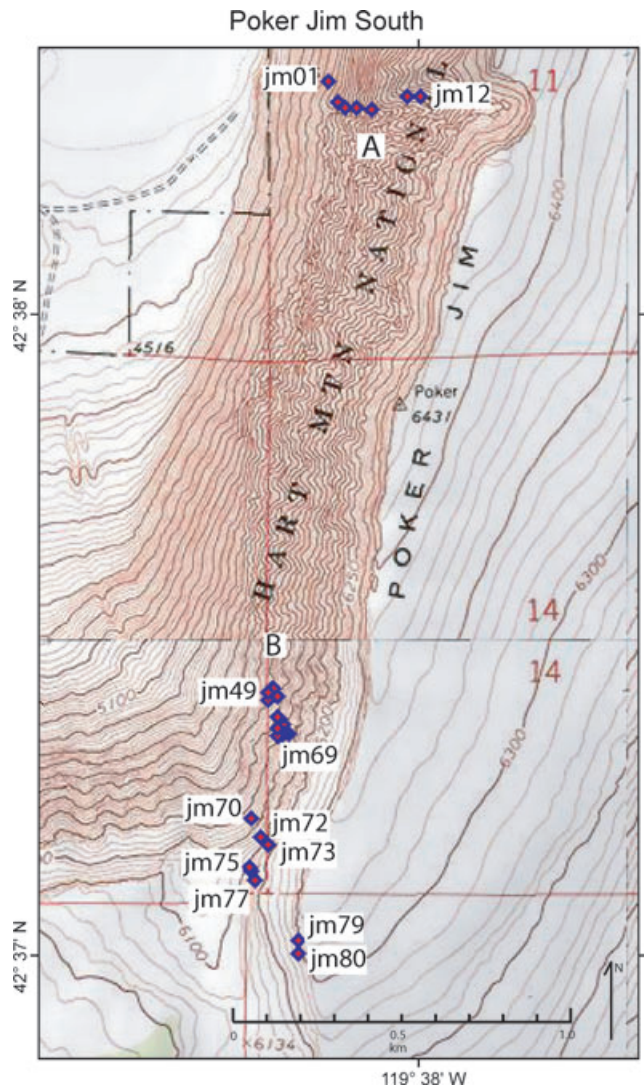


Figure 10. Flow locations for the Poker Jim South A and B sections. Only GPS located flows are shown.

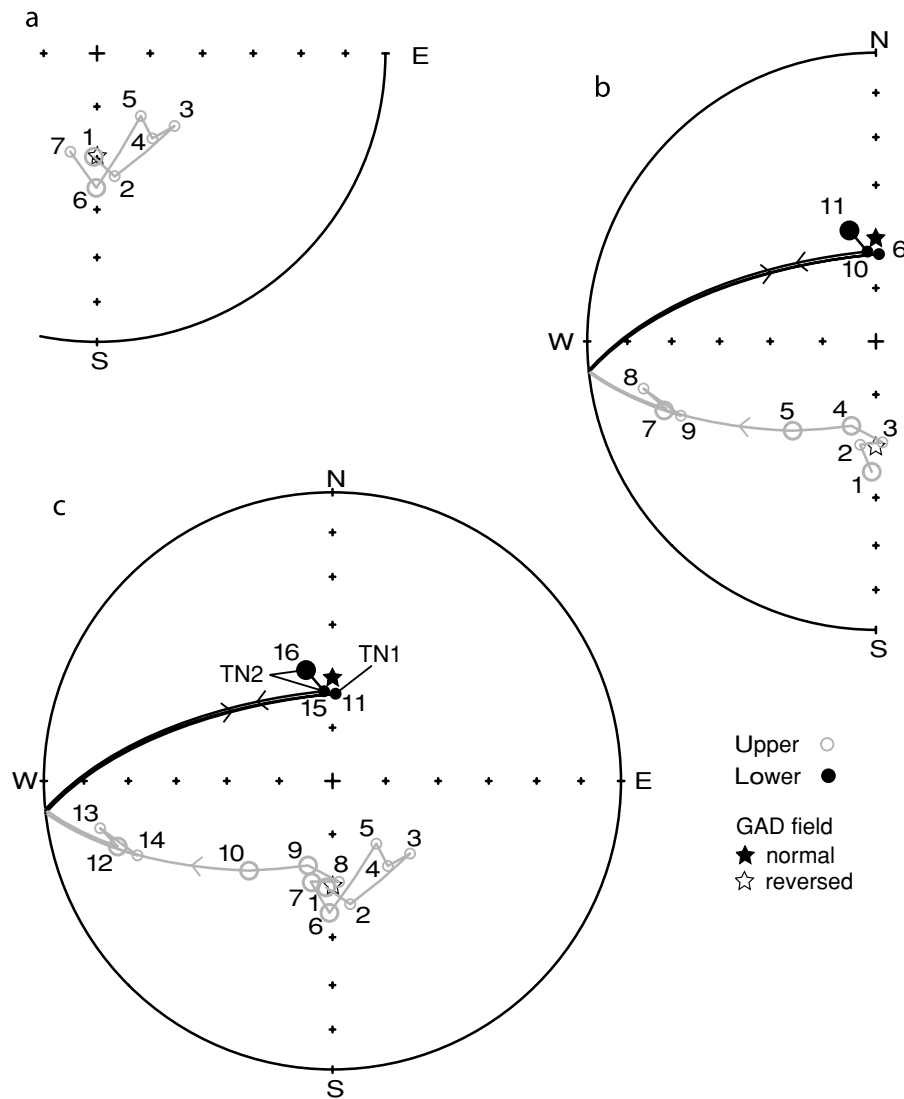


Figure 11. (a) Magnetic field directions of flow groups found at the Poker Jim South A section. (b) Flow group directions found at the Poker Jim South B section. (c) Flow groups combined and renumbered into one composite section. Note how 6 and 7 from (a) are similar to 1 and 2 from (b). Smaller symbols indicate flow groups consisting of a single flow. TN1 and TN2 are the first and second transitional normal groups, respectively.

10°. The section is flat-lying and no tilt corrections were made to the paleomagnetic directions (Table 1).

The paleomagnetic field directions found at Poker Jim North (Fig. 8) trace a path similar to the beginning of the field path found at Steens (Fig. 9a). The field in both cases starts from a stable reversed polarity direction, moves to a shallow south direction, then to a southeast and down direction, followed by the first temporary normal position (groups 29 and 30 for Steens and groups 9–17 for Poker Jim North). No other directions in the transitional path are found at Poker Jim North and thus it records only the beginning of the reversal. Goldstein *et al.* (1969) carried out a reconnaissance study at a location ~1 km southeast of our Poker Jim North section. The directional variation in the lower 80 per cent of their section, determined after 20 mT AF demagnetization of one or two specimens, roughly resemble ours.

3.2 Poker Jim South

The Poker Jim South sections (42.6°N, 119.6°W) are 88 km west of Steens Mountain at the south end of Poker Jim Ridge (Fig. 10). There

are two sections at the locality: section A with 12 sampled flows in the north and section B with 32 sampled flows 2 km to the south, which are combined into one composite section for the location. The sections are both flat-lying and no stratigraphic tilt correction have been applied to the paleomagnetic directions (Table 1).

Section A was sampled on a reconnaissance field trip when searching for the Steens reversal up a steep couloir in the Poker Jim Ridge cliff face (Supporting Information—Photos). Twelve flows were sampled out of approximately 65 flows in the 290 m section. Paleomagnetic laboratory analyses revealed that all of the flows have reversed polarity; the site was not revisited for further sampling. The flow groups for the section are shown in Fig. 11(a).

As section A was deemed too dangerous to continue collecting up to the top, section B was sampled on a later field trip. Thirty-two flows were drilled with only one exposed flow skipped at the 230 m section. Horizontal jogs were made in the sampling traverse (Fig. 10) to improve outcrop exposure and care was taken to trace flows laterally to ensure no exposed flows were missed. A few flows at the top of the section are likely not to have been sampled due to a lack of outcrop.

The paleomagnetic directions for flow groups for section B are shown in Fig. 11(b). The last two groups found in section A (6 and 7) have similar directions, and occur at the same elevations as the first two groups found in section B. We are therefore confident in combining the group directions into the single path shown in Fig. 11(c). Directional group 11 (flow jm72) seems possibly out of sequence, which could occur if a later-emplaced sill was mistaken for a lava flow; however, we do not believe this is the case as the unit was well exposed and was not recognized as a sill in the field. Moreover, the flow is not coarser grained than the other flows nearby, as would be expected for a more slowly cooled sill. A similar occurrence of a single unit with a different, seemingly out of sequence, direction was reported by Bogue & Coe (1982) in a Pliocene reversal transition on the Hawaiian island of Kauai. In this case, the unit was verified to be a lava flow when the location was revisited.

The combined Poker Jim South record documents a sequence of reverse, transitional and normal polarity directions that can be fit into a composite path of the Steens reversal. The transitional path does not have a compelling similarity to the Steens reversal, but it does visit a temporary normal polarity direction during the transition, as is also found in the Steens Mountain transitional record. Its proximity to the Poker Jim North section makes including its directions in the composite Steens reversal record a reasonable decision.

3.3 Catlow

The Catlow section (42.03°N, 118.33°W), which is located 68 km southeast of Steens Mountain, can be found down a ridge west of Catlow Peak (Fig. 12). This section was previously known to contain a magnetic reversal as described by Minor (1986) and was sampled in detail for this study. After our initial sampling, we returned to critical places in the section and drilled additional flows on both sides of the main sampling line where thin flows pinch out laterally and interfinger. Sixty-five flows were sampled from the 400 m section. Twenty flows were skipped, mostly at the bottom of the section where transitional flows were known, on the basis of fluxgate magnetometer measurements, not to be present. The section is tilted, with the flows on average striking 335° and dipping 12° to the east, as determined by Minor (1986) and confirmed during this study

with careful field measurements. A bedding tilt correction has been made to the Catlow section data in Table 1.

The Catlow directional groups (Fig. 13) are similar to the directions found at Steens (Fig. 9), although each section has unique directions that are not found at the other. Both Steens (S) and Catlow (C) records start with reverse polarity directions and move to a southeast and down direction (S35–S31, C15). Then both move to a temporary normal polarity direction (S30–S29, C16–C17) followed by a large number of directions in the northwest and down direction (S28–S22, C18–C27) before moving to the second temporary normal polarity direction (Steens N1 and N2, C29–C30). From there they both move back to the southeast and down direction (S21, C33–C35) before moving to the northeast and down (S16–S15, C36). Finally, they both finish the transition with secular variation around the expected normal polarity position (S14–S1, C37–C41).

4 EMPLACEMENT AND STRUCTURAL HISTORY OF SECTIONS BASED ON MAGNETIC STRATIGRAPHY AND SECULAR VARIATION

A detailed $^{40}\text{Ar}/^{39}\text{Ar}$ study of lavas that erupted during the Steens reversal yield a best age of $16.73 \pm 0.13/-0.08$ Ma (95 per cent confidence interval; Jarboe *et al.* 2010) determined with Bayesian statistics from the mean of the Steens reversal age and three other ages at the Catlow section. These lavas are thought to have erupted from dikes found in the Pueblo Mountains/Steens Mountain/Summit Springs escarpment (Mankinen *et al.* 1987). Dikes were not found at either the Catlow or Poker Jim Ridge sections, which support this view. We suggest that lavas erupted from the dikes found throughout the Steens escarpment from the Pueblo Mountains to the Summit Springs area, and that some of them flowed tens to a hundred kilometres over existing topography, eventually creating a relatively flat volcanic flow field. The lavas were later exposed by Basin and Range faulting, which started no earlier than 12 Ma (Colgan *et al.* 2006).

The transitional flows of the Steens reversal can be used as a time horizon across the Oregon Plateau in an area where other regional

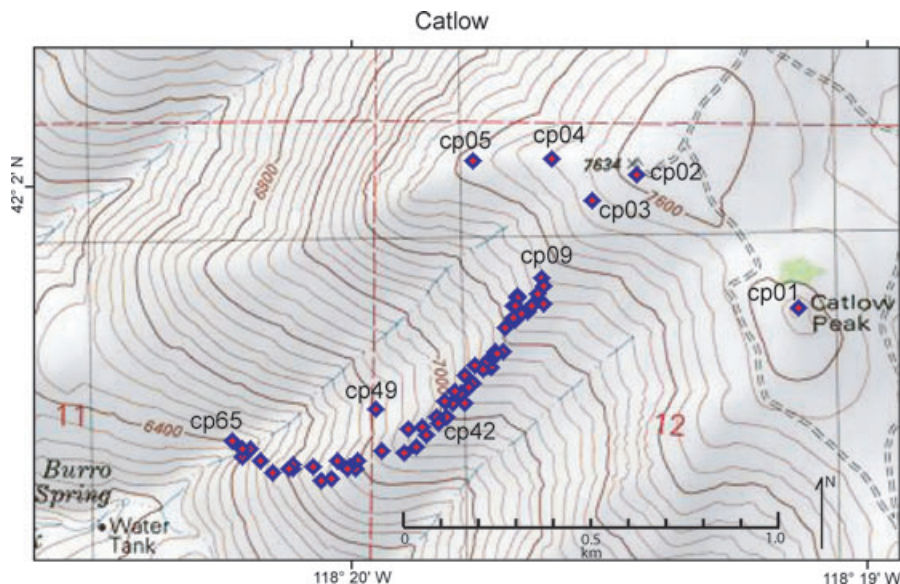


Figure 12. Flow locations at the Catlow section with selected flow IDs shown.

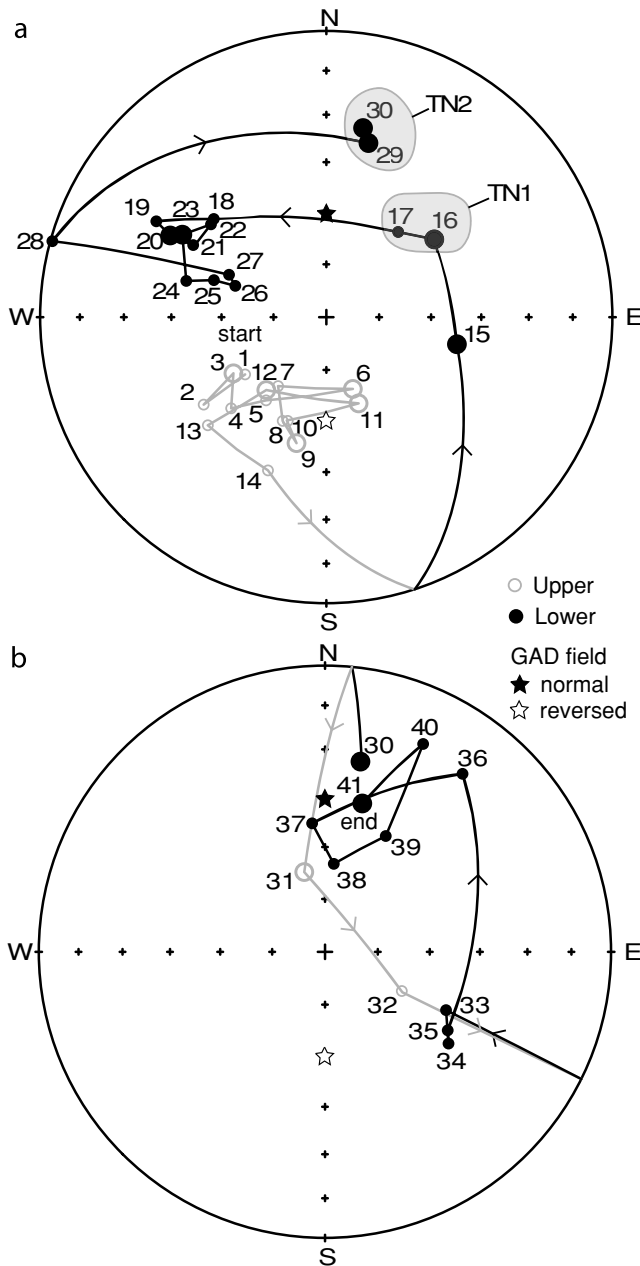


Figure 13. Magnetic field directional groups as found at the Catlow section shown in two parts. Figure (b) is a continuation of the path from (a). Smaller symbols indicate groups consisting of a single flow. TN1 and TN2 are the first and second transitional normal groups, respectively.

time markers are absent. In the southwest part of the field area, only reversed polarity flows are found at Guano Rim and Pueblo Mountains (Fig. 1), whereas in the middle of the field area transitional flows are found at Poker Jim, Steens Mountain and Catlow Peak. Further north at North Mickey and Summit Springs only normal polarity Steens basalts are present. This suggests that the source of the CRBG moved to the north as the eruptions proceeded, as advocated by Camp & Ross (2004).

4.1 Duration and rate of eruptions

Secular variation for the reversed polarity section at Poker Jim South suggests that the lavas there erupted over a short period of time. The

field directions are not disposed evenly around the expected reversed GAD field, but rather form a looping path off to one side with possibly a half loop on the other (Fig. 11c). This type of behaviour is seen in observatory records of the modern field and in studies of the recent paleomagnetic field recorded in archeologically and ¹⁴C-dated materials that carry thermoremanent magnetization (e.g. Ohno & Hamano 1992; Hagstrum & Champion 2002; Schnepp & Lanos, 2005). The reversed polarity part of the section sampled at Steens Mountain also has this looping behaviour (Fig. 8a) and was estimated by comparison to recent records of paleosecular variation to have erupted in 3100 ± 600 yr by Mankinen *et al.* (1985). Jarboe *et al.* (2008) used the same method to estimate the duration of Steens Basalt sections containing only full-polarity directions. Applying the method here, at Poker Jim South the reversed polarity section spans only 1.5–2.5 ka. At Catlow Peak the reversed polarity flow directions display two loops (Fig. 13, groups 1–6 and 7–13) that probably erupted in about 2–3 ka. At the top of the Catlow section there is also a single tight loop of the normal-polarity field, which suggests a brief span of order 1 ka. At none of the sections long hiatuses between eruptions seem to be present as no soil horizons were observed.

Using such secular variation arguments and the thickness of the transitional flows, Mankinen *et al.* (1985) estimated that the polarity transition lasted 3600–4400 yr at Steens Mountain. We can do the same for the Catlow and Poker Jim South sections presented here. At Catlow, we estimated that the normal and reversed polarity sections erupted in 2.5–3.5 ka. Those parts of the section have a combined thickness of 300 m (110 m of normal section and 190 m of reversed), which would give a mean eruption rate of 85–120 m ka⁻¹. Assuming that the transitional lavas at Catlow erupted at the same rate, their thickness of 105 m corresponds to 900–1200 yr. At Poker Jim South, 390 m of reverse polarity section erupted in 2–3 ka yielding a mean eruption rate of 130–195 m ka⁻¹. About half of the reversal is found at Poker Jim South in a section 80 m thick, corresponding to 800–1200 yr. Because of the few full polarity flows at Poker Jim North to enable recording of secular variation, eruption rates cannot be reasonably calculated. The durations of transitional lavas at the two sections are much shorter than the ~6 kyr estimated from sedimentary records for the average transition time of the last four reversals (from one full polarity directional state to the opposite) by Clement (2004) for mid-latitudes. This discrepancy is a possible indication of the large temporal gaps in the transition records of lava flow sections due possibly to the effects of episodic volcanism.

4.2 The composite directional record of the steens reversal

To combine the field directions from the three new sections into a composite record of the Steens reversal, we must be confident that the three sections with transitional field directions were erupted during the same reversal. Two lines of evidence indicate that this is the case: (i) the transitional field directions themselves are generally very similar and occur in the same sequence and (ii) ³⁹Ar/⁴⁰Ar ages of lava flows in the transition sections are of the same age. Jarboe *et al.* (2010) determined an age of 16.74 ± 0.36 Ma for Catlow transitional flow cp16, 16.53 ± 0.12 Ma for Poker Jim North transitional flow pj23, 16.67 ± 0.25 Ma for Steens transitional flow a40 and 16.61 ± 0.28 Ma for Steens transitional flow a41 (all uncertainties are one sigma unless otherwise stated). The error bounds for the ages of all these lava flows overlap, and a detailed analysis by Jarboe *et al.* (2010) makes a strong case that they all erupted during the same reversal.

Table 2. Summary of transitional directional groups found in the Steens reversal composite path. Steens transitional groups as defined by Prevot *et al.* (1985).

Transitional group number	Flow group	Flow IDs	<i>N</i>	<i>D</i> ^o	<i>I</i> ^o	<i>k</i>	α_{95}°	Long ^o	Lat ^o	dp ^o	dm ^o	<i>A</i> ₉₅ ^o	Rotated to North America			
													<i>D</i> ^o	<i>I</i> ^o	Long ^o	Lat ^o
1	S43	a66-69 b66-68	63	220.4	-47.2	122	1.6	161.8	-54.5	1.3	2.1	1.7	205.9	-47.2	177.2	-64.7
2	C14	cp43	7	200.8	-42.2	271	3.7	190.8	-65.4	2.8	4.5	3.5	186.3	-42.2	223.2	-71.6
3	PN3	pj6-11	48	199.7	-35.4	161	1.6	198.6	-61.5	1.1	1.8	1.4	185.2	-35.4	228.1	-66.4
4	S42	c65	8	199.2	-21.7	148	4.6	205.9	-54.8	2.6	4.9	3.6	184.7	-21.7	232.6	-58.4
5	S41	b65	6	183.8	-16.2	564	2.8	234.9	-55.5	1.5	2.9	2.1	169.3	-16.2	259.8	-54.4
6	S40	b64	7	184.7	-11.8	369	3.2	233.8	-52.1	1.7	3.3	2.4	170.2	-11.8	257.5	-52.3
7	S39	a65	10	184.5	-8.1	265	3.0	234.3	-51.2	1.5	3.0	2.1	170.0	-8.1	257.2	-50.5
8	S38	a64	12	181.0	-0.6	48	6.3	239.9	-47.7	3.2	6.3	4.5	166.5	-0.6	261.0	-46.0
9	S37	b63	7	175.7	-3.6	29	11.4	248.0	-49.0	5.7	11.4	8.1	161.2	-3.6	269.0	-45.9
10	PN4	pj12a	5	169.2	-16.0	217	5.6	258.9	-54.2	3.0	5.8	4.2	154.7	-16.0	280.5	-48.9
11	S36	a63	8	155.4	10.3	56	7.5	272.8	-37.2	3.8	7.6	5.4	140.9	10.3	288.2	-30.5
12	PN5	pj12b-14	15	136.9	6.8	222	2.6	292.1	-29.7	1.3	2.6	1.8	122.4	6.8	304.7	-20.7
13	PN6	pj15	8	139.1	14.2	87	6.0	287.6	-27.8	3.1	6.1	4.3	124.6	14.2	300.3	-19.2
14	S35	b61-62	9	134.1	12.4	194	3.7	293.9	-25.8	1.9	3.8	2.7	119.6	12.4	305.9	-16.7
15	S34	a62	5	122.5	40.9	43	11.8	292.4	-5.4	8.7	14.3	11.2	108.0	40.9	302.4	3.5
16	S33	a61, b60	13	134.9	35.7	169	3.2	285.1	-15.1	2.1	3.7	2.8	120.4	35.7	296.3	-7.0
17	S32	b59	7	140.7	29.6	97	6.1	282.2	-21.3	3.7	6.7	5.0	126.2	29.6	294.4	-13.5
18	S31	b52-58	36	143.4	36.1	117	2.2	277.7	-18.9	1.5	2.6	2.0	128.9	36.1	289.7	-11.7
19	PN7	pj16-21	47	152.1	38.6	145	1.7	268.1	-20.6	1.2	2.0	1.5	137.6	38.6	280.7	-14.6
20	PN8	pj22-24	23	142.0	47.3	58	4.0	273.8	-10.7	3.4	5.2	4.2	127.5	47.3	284.8	-4.0
21	C15	cp42-36	53	101.7	51.5	145	1.6	300.1	13.2	1.5	2.2	1.8	87.2	51.5	308.2	22.8
22	C16	cp35-34	15	54.1	51.7	94	4.0	326.2	46.6	3.7	5.5	4.5	39.6	51.7	335.7	57.3
23	C17	cp33	8	40.4	58.0	108	5.4	324.2	59.3	5.9	8.0	6.9	25.9	58.0	332.7	70.1
24	PN-9	pj25	7	24.3	61.8	65	7.7	321.1	72.2	9.2	11.9	10.5	9.8	61.8	324.7	82.8
25	PN10	pj26	8	27.0	51.0	228	3.7	348.7	66.0	3.4	5.0	4.1	12.5	51.0	14.3	75.2
26	PN11	pj27	8	22.9	58.5	68	6.7	334.1	72.4	7.4	9.9	8.6	8.4	58.5	356.4	82.8
27	PN12	pj28	8	35.0	80.9	70	6.7	258.7	56.0	12.5	12.9	12.7	20.5	80.9	252.3	58.9
28	PN13	pj29-32	29	31.2	68.0	167	2.1	297.9	67.3	3.0	3.5	3.2	16.7	68.0	288.3	75.9
29	PN14	pj33-35	24	31.8	75.0	113	2.8	273.9	63.2	4.7	5.1	4.9	17.3	75.0	262.7	68.3
30	S30	b51	5	352.5	81.1	11	23.6	237.0	59.8	44.0	45.6	44.8	338.0	81.1	229.1	58.2
31	PN15	pj36	8	342.6	74.3	95	5.9	216.0	69.2	9.7	10.7	10.2	328.1	74.3	204.6	63.8
32	PN16	pj37-39	24	340.2	47.0	167	2.3	114.6	68.4	1.9	3.0	2.4	325.7	47.0	134.0	58.8
33	PN17	pj40	6	343.6	62.6	133	6.1	162.1	78.0	7.5	9.5	8.4	329.1	62.6	164.3	67.6
34	PS11	jm72	8	2.0	65.3	202	3.9	256.2	85.0	5.1	6.3	5.7	347.5	65.3	183.2	80.0
35	S29	a57-60 b50	36	338.8	57.8	118	2.2	144.1	73.4	2.4	3.2	2.8	324.3	57.8	154.8	62.8
36	S28	a50-56 b40-49	95	299.3	48.8	164	1.1	157.2	40.4	1.0	1.5	1.2	284.8	48.8	165.8	29.9
37	S27	a49	5	315.9	58.6	213	5.3	160.8	56.9	5.8	7.9	6.8	301.4	58.6	167.7	46.5
38	C18	cp32	6	311.1	46.7	111	6.7	148.2	48.2	5.6	8.6	6.9	296.6	46.7	157.7	37.4
39	C19	cp31	8	299.4	32.4	42	8.8	145.6	33.4	5.6	9.9	7.4	284.9	32.4	155.5	22.6
40	C20	cp30-29	16	297.6	38.4	104	3.7	150.7	34.5	2.6	4.4	3.4	283.1	38.4	160.0	23.8
41	C21	cp28	7	298.4	46.5	27	12.4	156.5	38.7	10.2	15.9	12.7	283.9	46.5	165.1	28.0
42	C22	cp27	8	308.8	47.1	172	4.2	150.3	46.6	3.5	5.4	4.3	294.3	47.1	159.5	35.9
43	C23	cp26-24	24	299.8	41.6	49	4.3	151.5	37.5	3.2	5.3	4.1	285.3	41.6	160.7	26.8
44	C24	cp23	7	284.5	48.1	278	4.0	166.0	29.2	3.4	5.2	4.2	270.0	48.1	174.2	19.0
45	C25	cp22	9	288.2	56.0	26	10.7	171.5	35.8	11.0	15.4	13.0	273.7	56.0	178.7	25.9
46	C26	cp21	8	289.0	62.5	815	1.9	179.4	39.6	2.3	3.0	2.6	274.5	62.5	185.3	30.4
47	C27	cp20	8	293.5	59.6	140	4.7	173.5	41.3	5.3	7.1	6.1	279.0	59.6	179.9	31.5
48	S26	a48	16	281.5	58.7	230	2.4	177.1	32.9	2.7	3.6	3.1	267.0	58.7	184.1	23.6
49	S25	a47 b38-39	21	276.8	55.1	174	2.4	175.7	27.7	2.4	3.4	2.9	262.3	55.1	183.4	18.3
50	S24	a43-46 b36-37 f4-6	62	279.8	49.0	95	1.9	168.8	26.5	1.7	2.5	2.1	265.3	49.0	177.1	16.6
51	S23	a42	8	270.5	52.6	39	8.9	176.8	22.1	8.4	12.3	10.2	256.0	52.6	185.0	12.8
52	S22	a41	8	267.0	62.4	18	13.3	187.0	27.3	16.2	20.7	18.3	252.5	62.4	195.0	17.9
53	PS12	jm73-74	13	253.0	-23.3	161	3.4	152.8	-20.7	1.9	3.6	2.6	238.5	-23.3	163.3	-31.2
54	PS13	jm75	8	258.5	-19.0	393	2.9	150.9	-15.0	1.6	3.0	2.2	244.0	-19.0	161.1	-25.6
55	PS14	jm76	7	249.1	-28.5	85	7.3	153.0	-25.5	4.4	8.0	5.9	234.6	-28.5	163.7	-36.1
56	C28	cp19	7	285.5	0.8	101	6.1	141.5	11.7	3.1	6.1	4.3	271.0	0.8	151.3	1.0
57	PS15	jm77	8	354.6	64.5	309	3.2	196.5	84.6	4.1	5.1	4.6	340.1	64.5	172.1	75.4
58	PS16	jm78-80	24	346.6	57.6	222	2.0	131.7	78.9	2.1	2.9	2.5	332.1	57.6	148.2	68.4
59	N1	b34-35 f3	36	12.8	40.3	222	1.6	28.9	67.7	1.2	1.9	1.5	358.3	40.3	66.1	70.3
60	C29	cp18-16	23	13.6	37.5	433	1.5	28.9	66.1	1.0	1.8	1.3	359.1	37.5	64.0	69.0
61	C30	cp15-15b	19	11.0	33.2	212	2.3	36.9	64.3	1.5	2.6	2.0	356.5	33.2	69.9	65.9
62	N-2	b33	12	329.9	43.3	100	4.4	125.9	59.8	3.4	5.5	4.3	315.4	43.3	140.5	49.7
63	C31	cp14a-14	21	345.4	-66.5	36	5.4	71.2	-1.9	7.3	8.9	8.1	330.9	-66.5	80.4	-4.5

Table 2. (Continued.)

Transitional group number	Flow group	Flow IDs	<i>N</i>	<i>D</i> [°]	<i>I</i> [°]	<i>k</i>	α_{95} [°]	Long [°]	Lat [°]	dp [°]	dm [°]	<i>A</i> ₉₅ [°]	Rotated to North America			
													<i>D</i> [°]	<i>I</i> [°]	Long [°]	Lat [°]
64	C32	cp13a	6	117.6	−65.1	152	5.8	0.7	−46.4	7.6	9.4	8.5	103.1	−65.1	5.4	−37.2
65	S21	a38-40 b29-32 f2	67	142.7	33.8	90	1.8	279.1	−19.9	1.2	2.1	1.6	128.2	33.8	291.2	−12.5
66	C33	cp13	7	115.7	51.2	72	7.3	291.8	4.6	6.7	9.9	8.1	101.2	51.2	300.6	13.3
67	C34	cp12	8	126.6	45.3	143	4.7	287.7	−5.4	3.8	6.0	4.8	112.1	45.3	297.6	3.0
68	C35	cp11	8	122.6	47.8	40	9.3	289.3	−1.6	7.9	12.1	9.8	108.1	47.8	298.7	6.9
69	S20	a37	7	64.4	−27.6	248	3.8	359.7	7.8	2.3	4.1	3.1	49.9	−27.6	10.8	16.7
70	S19	a35-36 b28	16	60.4	−23.3	230	2.4	0.9	12.3	1.4	2.6	1.9	45.9	−23.3	12.6	21.0
71	S18	a34	5	58.7	−16.5	702	2.9	359.8	16.2	1.5	3.0	2.1	44.2	−16.5	11.8	25.0
72	S17	a33	5	50.2	−10.1	83	8.5	4.4	24.2	4.4	8.6	6.2	35.7	−10.1	17.9	32.4
73	S16	a31-32 b26-27	26	39.9	15.2	319	1.6	4.6	40.6	0.8	1.6	1.1	25.4	15.2	21.4	48.6
74	C36	cp10	8	37.7	22.5	20	14.3	3.3	45.4	8.0	15.2	11.0	23.2	22.5	21.2	53.6
75	S15	a30	6	31.6	37.5	239	4.3	0.8	55.9	3.0	5.1	3.9	17.1	37.5	22.5	64.1

Flow mean directions were calculated using PMGSC4.2 software by R. Enkin. VGPs calculated using PaleoMac by J.P. Coe. Sections are flat-lying except for Catlow where the data were corrected for a tilt striking 335° dipping 12°E. Flow ID, label given the flow(s) in the field; *N*, number of specimens used to determine mean flow group direction; *D* (*I*), mean magnetic declination (inclination) of the flow group; *k*, precision parameter of the mean direction; α_{95} , 95 per cent confidence limit on the mean direction; Long (Lat), latitude (longitude) of the virtual geomagnetic pole (VGP); *A*₉₅, 95 per cent confidence limit on the VGP.

during the temporary normal polarity episode within the transition. Secular variation of the full polarity field after the transition shows a more regular sequential progression and looping as documented by Mankinen *et al.* (1985) and Jarboe *et al.* (2008). In addition, the jump from PN8 with a southeast and downward direction to PN9–PN14 with northeast and downward directions is reinforced by the similar directional behaviour in the more detailed Catlow record groups C15–C17 as the field moved to the first temporary normal polarity direction.

4.5 Poker Jim South

Placement of some of the magnetic field directions recorded at the Poker Jim South (PS) section are the least constrained part of splicing the various fragmentary records of the Steens reversal. The following interpretation introduces minimum complexity into the composite path. The directions in the lower 350 m of the section represent secular variation of the reversed polarity magnetic field leading up to the Steens reversal (Fig. 11). The upper 100 m records the first temporary normal polarity position, some new transitional directions and the second temporary normal polarity position (Fig. 11c). At the top of the reversed section, moving toward the transition, the first direction PS10 is placed (Fig. 14) between PN1 and PN2. The swing of the field to the southeast and downward direction is missing at the Poker Jim South section, and the next direction (PS11) is in the first temporary normal polarity position between PN17 and S29. The next three groups, PS12–P14, are west and upward, a direction not found at any of the other sections. They are placed after S26 and before C28, between the west and downward and the second temporary normal polarity cluster. The final two directions found at Poker Jim South, PS15 and P16, are placed in the second temporary normal polarity position after C28 and before Steens N1.

To summarize the composite record, all of the transitional group directions have been placed in order in Table 2. The earlier records from Steens Mountain (Prevot *et al.* (1985); Camps *et al.* 1999) had 30 transitional directional groups. Our transitional directions are those placed in transitional sequence after the first transitional direction and before the last transitional direction as defined by Prevot *et al.* (1985). We have added 45 new groups, to provide a total of 75 directional groups to describe the Steens Mountain polarity transition.

4.6 The composite VGP path of the steens reversal

To compare the Steens polarity transition with other transition records it is useful to express the composite directional path in terms of VGPs. The Steens reversal VGP path (Fig. 15) starts south of Australia (PN1), then moved east to a first cluster of directions around western South America (PN5–PN6, S35–S31, PN7–PN8, C15), then it moved to and around the first transitional normal polarity position (TN1). Next the VGPs moved south to a cluster of directions in the western Pacific off the coast of Japan (C18–C27, S26–S22) before moving on to three directions close to eastern Australia (PS12–PS14). The path then moved to and around the second transitional normal polarity position (TN2) before looping through the Indian (C31) and South Atlantic (C32) Oceans. Next it moved back to the cluster around western South America (S21, C33–C35). The directions finally swung over to western Africa (S20–S16) and moved north to the end of the reversal. As discussed later in the paper, the Oregon Plateau has rotated 14.5° clockwise with respect to cratonic North America. As shown in Fig. 16, correcting the VGP path for this rotation does not affect any of the observations mentioned earlier.

5 DISCUSSION

Whether some, most or all polarity transitions are simple or complex has been discussed for 40 yr and still remains an issue (Coe & Glen 2004). The original (Watkins 1969) and later ‘benchmark’ (Mankinen *et al.* 1985) directional record of the Steens Mountain reversed (R) to normal (N) polarity reversal consisted of two transitional (T) phases separated by a temporary normal polarity interlude. It can be described in shorthand as R-T-N-T-N. Much of the transition path consisted of clusters of directions separated by gaps of about 60°, 70° and 100°, which raises the question of whether this appearance indicates stop-and-go transitional field behaviour or episodic volcanism. If the former, then the eruption of some lavas with clustered directions would have spanned considerable transitional time and some of the gaps would mark episodes of rapid field motion. The composite transition path is longer and more complex: now it can be described as R-T-N-T-N-T-R-T-N (Fig. 14). The first gap of 60° is divided into two roughly equal halves, the second gap of 70° is now replaced by the entirely new T-N-T-R-T part of the transition record that has five new gaps of 90°, 40°, 80°,

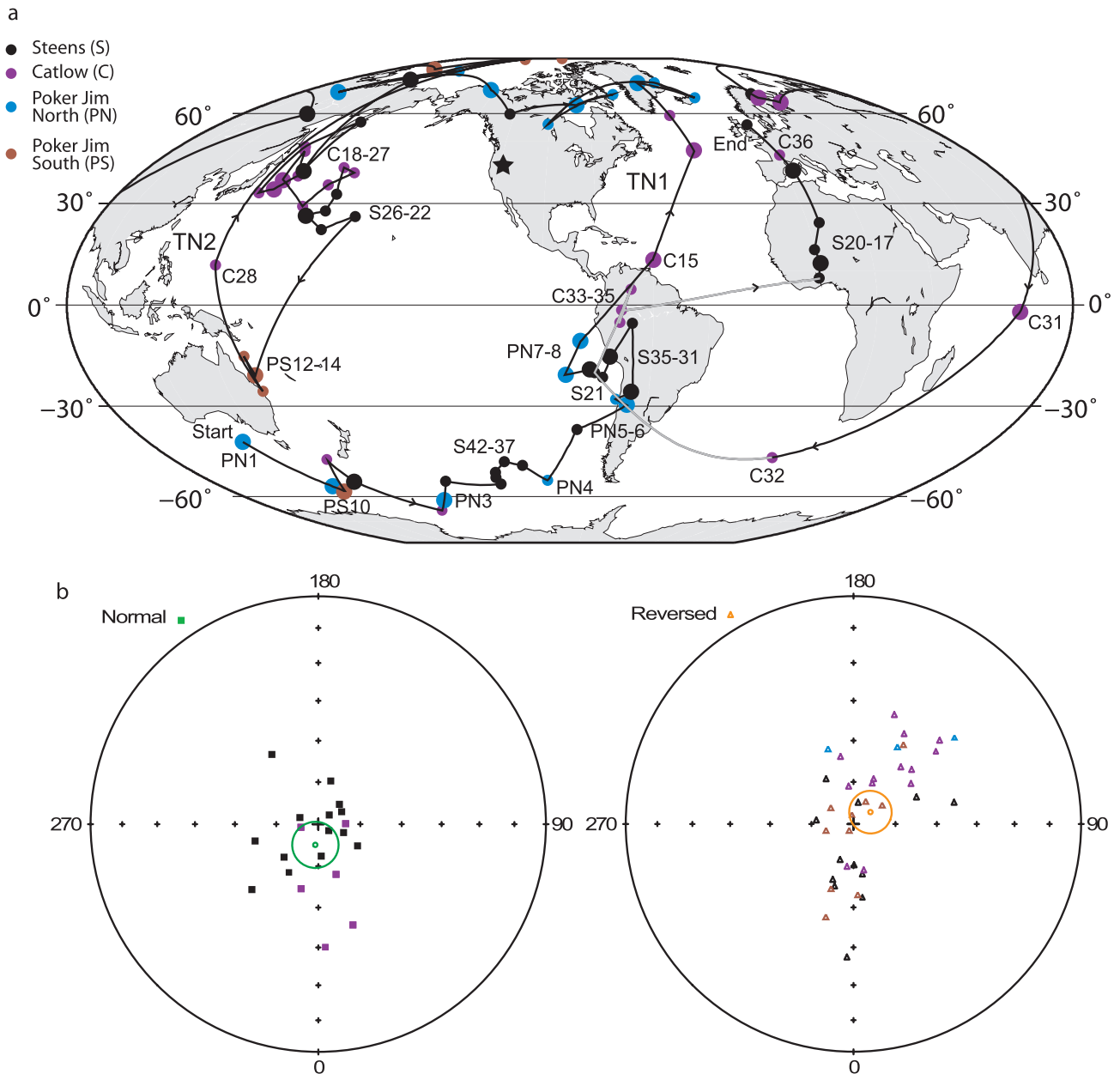


Figure 15. (a) VGPs of the composite path of the Steens reversal. Numbers indicate directional group IDs. TN1 marks the first visit to normal polarity during the reversal. TN2 marks the second movement to normal polarity. Star marks the study area locality. Smaller directional group symbols indicate a group consisting of a single flow. (b) VGPs of the normal and reversed non-transitional directions from Steens, Catlow and Poker Jim. For the normal VGPs: longitude = 352.1, latitude = 82.5, A_{95} = 8.2°. For the reversed VGPs: longitude = 124.9, latitude = -82.6, A_{95} = 7.6°.

150° and 100°, and the third gap is little changed. With regard to the hypothesis of extremely rapid field change in the gaps of the benchmark Steens record (Mankinen *et al.* 1985; Coe & Prévot 1989; Camps *et al.* 1995; Coe *et al.* 1995), which was based on anomalously streaked intraflow scattering of specimen ChRM directions associated with gaps one and two, it is still a possibility for the first gap, it is clearly not the case for the second gap, and no additional evidence has been obtained with regard to the third gap.

The composite Steens transition has four clusters of directions with VGP latitudes less than 45° from the equator: two highly populated clusters around western South America (WSA) and the western Pacific (WPA), and two lesser ones near the east coast of Australia (EAU) and in western Africa (WAF). Only one (EAU) was not

present in the benchmark record from Steens Mountain. The direct method of solving whether the clusters of directions are due to standstills in field motion rather than to episodic volcanism would be to date the lavas to high enough precision. This would require a resolution on the order of a few hundred years, while the best dating methods for these ~16.7 Ma, low-potassium basalts give a precision of not better than 100 ka (Jarboe *et al.* 2010). Other methods are needed to address the issue. The WPA cluster is represented in both the Steens Mountain and Poker Jim sections, and the WSA is recorded at all three localities. These sections are separated from each other by 80–100 km, and each cluster contains flows that differ significantly in chemistry, both within and between sections (manuscript in preparation). These characteristics seem more consistent with each directional cluster spanning considerable time

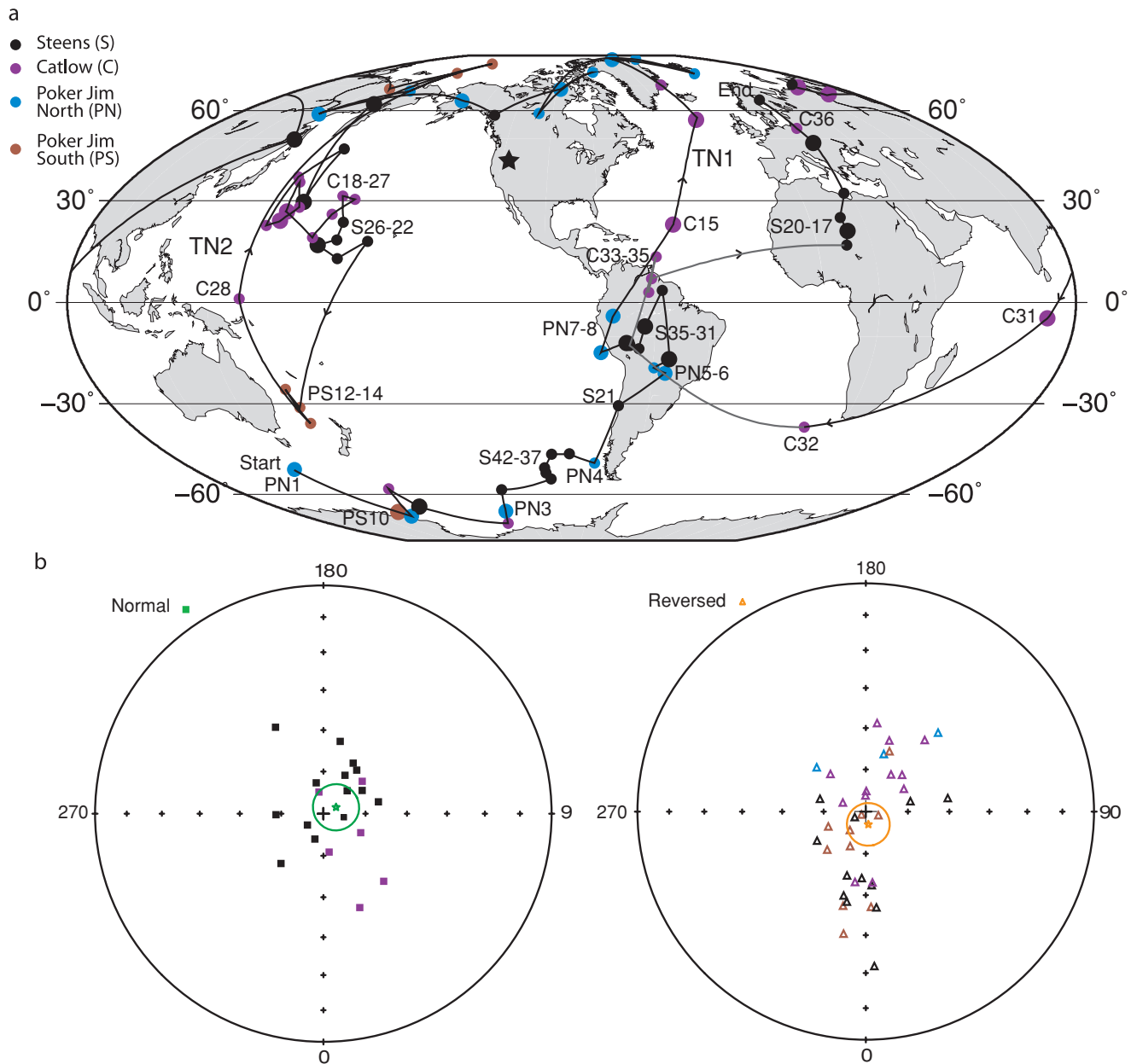


Figure 16. (a) VGPs of the composite path of the Steens reversal where the directions have been rotated back to stable North America. Numbers indicate directional group IDs. TN1 marks the first visit to normal polarity during the reversal. TN2 marks the second movement to normal polarity. Star marks the study area locality. Smaller directional group symbols indicate a group consisting of a single flow. (b) VGPs rotated back to stable North America of the normal and reversed non-transitional directions from Steens, Catlow and Poker Jim. For the normal VGPs: longitude = 111.7, latitude = 84.9, $A_{95} = 8.2^\circ$. For the reversed VGPs: longitude = 111.3, latitude = -85.3 , $A_{95} = 7.6^\circ$.

rather than arising from brief random bursts of volcanism. Paleointensity studies also support this view as some directions in the clusters remained the same as the intensity changed considerably (Prevot *et al.* 1985). Even more persuasive, the WSA cluster is visited twice, both early and late in the transition, the first time in the Steens and Poker Jim records and the second time in the Steens and Catlow records.

The revisitation of the WSA cluster and probable lingering of transitional VGPs both times at this location suggest a geographical preference, perhaps controlled by conditions at the core–mantle boundary. The clumps of directions could be a signal of high heat flow at the CMB due to subduction of cold slabs under South America, consistent with tomographic images of the lowermost mantle in

which high seismic shear-wave velocity occur (Grand 2002). This idea is strengthened by some numerical dynamo simulations, which produce bundles of steeply inclined magnetic flux and resulting high transitional VGP density due to downwelling of core fluid at regions of higher than average CMB heat flow (Olson & Christensen 2002; Kutzner & Christensen 2004). Further support for a statistical South American VGP preference is afforded by some other transition records: the Matuyama-Brunhes precursor record from La Palma (Singer *et al.* 2002), the Kamikatsura event from Maui (Coe *et al.* 2004) and the Gilsa event from Lanai (Leonhardt *et al.* 2009).

The WPA and EAU VGP clusters in the Steens transition record also overlie deep mantle regions of high shear-wave velocity

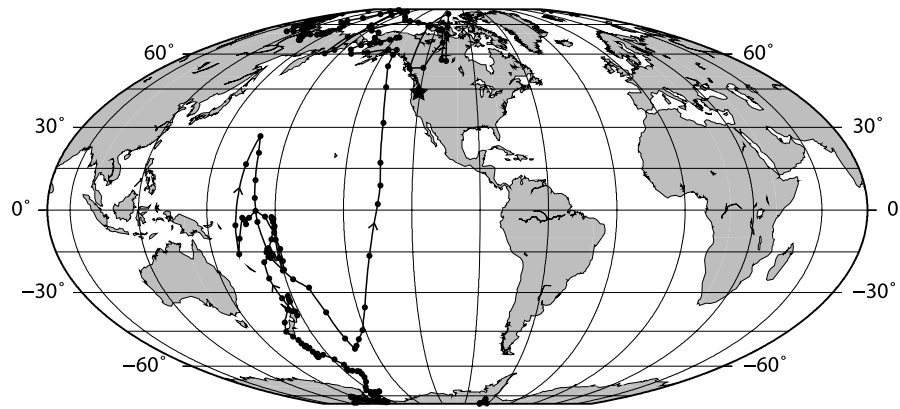


Figure 17. VGPs from the Matuyama-Brunhes transition, calculated from the model of Leonhardt & Fabian (2007) as seen from Steens Mountain (star).

Table 3. Direction and VGP directional group means for the three new localities, other locations on the Oregon Plateau from Jarboe *et al.* (2008), and Steens Mountain, plus various reference poles.

Pole locations	<i>N</i>	<i>D</i> °	<i>I</i> °	<i>k</i>	α_{95} °	Long°	Lat°	<i>K</i>	<i>A</i> ₉₅ °	<i>S</i>	<i>S</i> -	<i>S</i> +
Poker Jim (pj,jm) ^d	13	187.9	-61.1	20.3	9.4	143.5	-84.9	10.3	13.6	25.2	-9.3	5.4
Catlow Normal (cp)	6	20.1	44.1	15.1	17.8	8.8	69.3	17.1	16.7	19.6	-11.3	5.2
Catlow Reversed (cp)	13	209.4	-59.6	31.0	7.6	146.7	-68.6	16.4	10.6	20.0	-7.4	4.2
Catlow All (cp) ^b	19	25.8	54.9	20.5	7.6	337.4	70.1	15.3	8.9	20.7	-5.8	3.7
Steens Normal ^c	14	4.0	61.9	42.9	6.1	304.1	86.7	21.0	8.9	17.7	-6.0	3.6
Steens Reversed ^c	12	168.4	-65.2	27.1	8.5	10.4	-79.9	12.5	12.8	22.9	-8.5	4.9
Steens All ^{b,c}	26	357.3	63.6	32.6	5.0	213.8	85.8	15.4	7.5	20.7	-5.4	3.3
Oregon Plateau (Jarboe <i>et al.</i> 2008) ^d	76	5.4	60.8	25.6	3.3	318.4	85.7	15.1	4.3	20.8	-2.4	2.2
Oregon Plateau (this paper) ^e	108	9.8	60.1	22.6	2.9	328.1	82.9	13.6	3.8	22.0	-2.3	1.9
High Plains ^c	28					209.0	88.3	19.9	6.3	18.2	-4.7	2.9
CRBG ^f	59					171.6	88.7	22.9	4.0	16.9	-2.5	1.9
North American Plate ^g	25					147.0	86.3		2.7			

N, number of sites in the mean; Long (Lat), longitude (latitude) of the VGP mean; *K*, precision parameter of the mean VGP; *A*₉₅, 95 per cent confidence limit on the VGP mean; *S*, angular dispersion, *S*-(+), 95 per cent negative (positive) confidence interval of the angular dispersion determined from Cox (1969).

^aDirections from Poker Jim North and South combined.

^bThe antipodes of reversed polarity flows used.

^cMankinen *et al.* (1985) DGs 1–14 (normal) and 44–55 (reversed) as determined in Prevot *et al.* (1985).

^dMean from all non-transitional groups at Steens, ss, pm, nm and gr.

^eMean from all of Jarboe *et al.* (2008) and all non-transitional groups at pj, jm and cp.

^fColumbia River Basalt Group Mean from flows selected by Mankinen *et al.* (1987).

^g16.7 Ma (interpolated) synthetic reference pole from Torsvik *et al.* (2008).

associated with subduction zones along the western Pacific margin (Grand 2002). The Matuyama-Brunhes record from Maui (Coe *et al.* 2004) has a prominent VGP cluster just east of New Zealand, and the model of Leonhardt & Fabian (2007) for that reversal predicts a VGP path along the western Pacific, from high southern latitudes up to 25°N and back again to 40°S (Fig. 17). Other VGP clusters around Australia are observed in records of the Matuyama-Brunhes precursor from Tahiti (Chauvin *et al.* 1990) and from Chile (Brown *et al.* 2004) and the Gilsa event (Leonhardt *et al.* 2009). The fourth Steens cluster WAF, however, overlies slow, presumably hotter lower mantle, although it is also represented by VGP clusters in several records, including the Gauss-Matuyama transition in Searles Lake sediments (Glen *et al.* 1999) and the Gilbert-Gauss and Lower Mammoth transitions in lavas from Oahu (Herrero-Bervera & Coe 1999).

In summary, the composite Steens reversal path supports the notion that VGPs of transitions recorded in western North America lie preferentially in the two rather broad longitudinal bands, specifically those of Glen *et al.* (1999) described earlier. It also provides some support for stop-and-go transitional field behaviour in which

the VGP tends to linger near preferred geographical. But the directional variation becomes more complex as new sections are added, consistent with suggestions that many reversals may be significantly more complex than are currently depicted in both sedimentary and lava-flow records (Channell & Lehman 1997; Coe & Glen 2004).

6 ROTATION OF THE OREGON PLATEAU

Our data from the three sections provide additional poles that support the conclusion of Jarboe *et al.* (2008) that the Oregon Plateau has rotated clockwise relative to the CRBG and cratonic North America. Jarboe *et al.* (2008) used 50 directional groups from sections at Summit Springs, North Mickey, Pueblo Mountains and Guano Rim (Fig. 1) together with 26 non-transitional directional groups for Steens Mountain. Our additional 32 non-transitional group directions from Catlow, Poker Jim North and Poker Jim South redefine an already high-quality paleomagnetic pole for the Oregon Plateau (Table 3) that is rotated more in the clockwise direction by

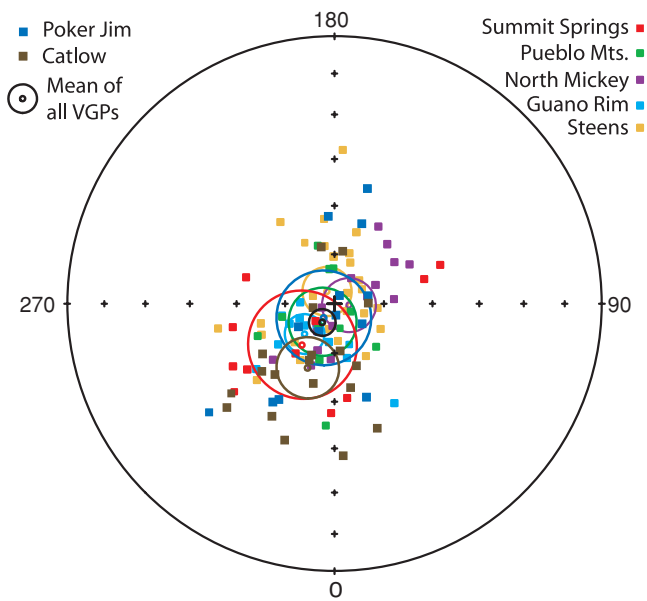


Figure 18. Site-mean north virtual geomagnetic poles for stable directions at Catlow, Poker Jim Ridge, the four localities of Jarboe *et al.* (2008) and Steens Mountain (Mankinen *et al.*, 1985). Locality-mean poles and corresponding circles of 95 per cent confidence interval are shown. Mean direction statistics: Poker Jim ($N = 13$, $D = 187.9$, $I = -61.1$, $\alpha_{95} = 9.4$), Catlow ($N = 19$, $D = 25.8$, $I = 54.9$, $\alpha_{95} = 7.6$), Summit Springs ($N = 11$, $D = 18.6$, $I = 60.0$, $\alpha_{95} = 13.4$), Pueblo Mts. ($N = 11$, $D = 190.2$, $I = -59.9$, $\alpha_{95} = 8.3$), North Mickey ($N = 16$, $D = 356.9$, $I = -58.7$, $\alpha_{95} = 6.0$), Guano Rim ($N = 12$, $D = 197.4$, $I = -58.7$, $\alpha_{95} = 8.0$), Steens ($N = 26$, $D = 357.3$, $I = 63.3$, $\alpha_{95} = 5.0$).

3.9° (Fig. 18). In comparison to other estimates for the region, this new Oregon Plateau pole is rotated $11.0^\circ \pm 7.5^\circ$ clockwise with respect to the Mankinen *et al.* (1987) High Plains pole, which consists almost exclusively of VGPs from Steens Mountain. The CRBG pole in Table 3 was also calculated by those authors and consists of 59 younger flows from the CRBG to the north in Washington and northern Oregon. With respect to this pole, our Oregon Plateau pole is clockwise rotated $11.4^\circ \pm 5.6^\circ$.

Present-day rotation rates by McCaffrey *et al.* (2007) are in reasonable agreement with this result. Their estimate of the rotation rate in eastern Washington is zero within error ($0.008^\circ \pm 0.016^\circ/\text{Ma}$) and thus is the same as assumed for the CRBG above. They inverted GPS velocities along with other geological rate markers and estimated that the Southeast Oregon (SEOr) block, on which all of the poles here for the Oregon Plateau are found, is rotating at a rate of $0.406^\circ \pm 0.021^\circ/\text{Ma}$ clockwise with respect to the CRBG or North America. Assuming this rate to be constant and using the age of the Steens reversal (16.72 Ma) as the mean age of the Steens lavas predicts a clockwise rotation of $6.8^\circ \pm 0.4^\circ$. This is a lower than our estimates, but within uncertainties of the paleomagnetic determination.

Other poles from North America, aside from the CRBG, are not available due to the lack of studies of volcanic eruptions around 10–20 Ma. By reconstructing the relative plate locations in the past using seafloor magnetic anomalies, data from other continents can be used to calculate a North American Pole. Torsvik *et al.* (2008) calculated such a synthetic pole for North America for 10 and 20 Ma, and the interpolated pole position for 16.7 Ma is given in Table 3. Relative to this pole the Oregon Plateau is clockwise rotated $14.5^\circ \pm 4.6^\circ$.

As described by Jarboe *et al.* (2008), earlier studies by Magill & Cox (1980, 1981) suggested that south-central Oregon was rotated about 10° clockwise relative to southeast Washington, but the High Plains result of Mankinen *et al.* (1987) ruled out this possibility. Our data together with those of Jarboe *et al.* (2008) indicate that clockwise rotation has likely occurred at a higher rate than found by McCaffrey *et al.* (2007). This suggests that the SEOr block in the McCaffrey *et al.* (2007) model was rotating more quickly in the past than at present.

7 CONCLUSIONS

Previous studies at Steens Mountain (Mankinen *et al.* 1985; Prevot *et al.* 1995; Camps *et al.* 1999) documented the most detailed record available from volcanic rocks of Earth's magnetic field behaviour during a geomagnetic polarity reversal. After grouping successive flows with insignificantly different directions, it comprised 30 transitional directional groups. Our study has significantly augmented that record with the addition of 45 directional groups for a total of 75 distinguishable transition directions, which confirms most parts of the earlier record but also reveals a more complex reversal history. The composite path derived by splicing the results from the three new sections with the earlier results from Steens Mountain is much longer, with new west and upward directions, adding another large, N-T-R-T swing of the transitional field, and filling in directions on the path between previously determined directional jumps. Major features of the VGP path include an augmented cluster in the western Pacific and a new one just east of Australia, a strong and multiply confirmed cluster around western South America that is visited twice, and a cluster in western Africa that continues northward into western Europe as stable normal polarity is established. The locations of these clusters and many of the more widely spaced VGPs are consistent with the two broad VGP bands evident in a compilation of western North American sedimentary and igneous records of the past 17 Ma (Glen *et al.*, 1999), which are shifted about 30° eastward of the global bands described earlier (Laj *et al.* 1991; Tric *et al.* 1991). Representation of these cluster locations in this and various other transition records and the statistical preference of the transitional VGPs for the bands is evidence for persistent features at the CMB such as topography, lower heat flow or chemical compositional differences that influence the flow of core fluid and the distribution of magnetic flux. Although the composite VGP path of the Steens reversal is consistent with longitudinal bands, in detail it contains large variations from these idealized structures and supports the generalization that individual VGP paths depend on the location of the observer and may vary greatly from reversal to reversal.

Detailed stratigraphic mapping and documentation of secular variation of the non-transitional geomagnetic field allows for the estimation of maximum eruption rates at two of the three new sections: $85\text{--}120 \text{ m ka}^{-1}$ at Catlow, and $130\text{--}195 \text{ m ka}^{-1}$ at Poker Jim South. These rates are maxima because they do not take into account intervals between eruptions that are too long to track secular variation. VGPs of non-transitional directions together with others on the Oregon Plateau define an improved pole for the area that indicates a clockwise rotation of $11.4^\circ \pm 5.6^\circ$ with respect to CRBG and $14.5^\circ \pm 4.6^\circ$ with respect to cratonic North America. This rotation contradicts earlier conclusions that the south-central Oregon plateau was stable relative to the North American interior since Early Miocene time but is consistent with a recent estimate of clockwise rotation rate based on GPS measurements.

ACKNOWLEDGMENTS

We thank Eli Morris and Walter Schillinger for paleomagnetic instrumentation and software support at UCSC. For highly competent field work assistance, we thank Mike Dueck, Bijan Hatami, Peter Lippert and Ariel Mendoza-Peñate. A review of this paper and helpful comments were given by Pierre Camps, Andrew Roberts and James Gill. Discussions with Chris Pluhar on software, hardware and analytical procedures were helpful. This work was funded by NSF grants EAR-0310316 and EAR-0711418 to RSC and JMG and minigrants from the UCSC Committee on Research and Institute of Geophysics and Planetary Physics.

REFERENCES

- Bogue, S.W. & Coe, R.S., 1982. Successive paleomagnetic reversal records from Kauai, *Nature*, **295**, 399–401.
- Brown, L.L., Singer, B.S., Pickens, J.C. & Jicha, B.R., 2004. Paleomagnetic directions and Ar-40/Ar-39 ages from the Tataro-San Pedro volcanic complex, Chilean Andes: lava record of a Matuyama-Brunhes precursor?, *J. geophys. Res.*, **109**, doi:10.1029/2004JB003007.
- Camp, V.E. & Ross, M.E., 2004. Mantle dynamics and genesis of mafic magmatism in the intermontane Pacific Northwest, *J. geophys. Res.*, **109**, doi:10.1029/2003JB002838.
- Camp, V.E., Ross, M.E. & Hanson, W.E., 2003. Genesis of flood basalts and basin and range volcanic rocks from Steens mountain to the Malheur River Gorge, *Bull. geol. Soc. Am.*, **115**, 105–128.
- Camp, V.E., Ross, M.E., Duncan, R.A., Jarboe, N.A., Coe, R.S., Hannan, B.B. & Johnson, J.A., 2011. The Steens Basalt: earliest lavas of the Columbia River Basalt Group, submitted.
- Camps, P., Coe, R.S. & Prévot, M., 1999. Transitional geomagnetic impulse hypothesis: geomagnetic fact or rock-magnetic artifact?, *J. geophys. Res.*, **104**, 17 747–17 758.
- Camps, P., Prévot, M. & Coe, R.S., 1995. Revisiting the initial sites of geomagnetic-field impulses during the Steens-Mountain polarity reversal, *Geophys. J. Int.*, **123**, 484–506.
- Channell, J.E.T. & Lehman, B., 1997. The last two geomagnetic polarity reversals recorded in high-deposition-rate sediment drifts, *Nature*, **389**, 712–715.
- Chauvin, A., Roperch, P. & Duncan, R.A., 1990. Records of geomagnetic reversals from volcanic islands of French-Polynesia. 2. Paleomagnetic study of a flow sequence (1.2–0.6 Ma) from the island of Tahiti and discussion of reversal models, *J. geophys. Res.*, **95**, 2727–2752.
- Clement, B.M., 1991. Geographical-distribution of transitional VGP—evidence for non-zonal equatorial symmetry during the Matuyama-Brunhes geomagnetic reversal, *Earth planet. Sci. Lett.*, **104**, 48–58.
- Coe, R.S. & Glen, J.M., 2004. The complexity of reversals, in: *Timescales of the Paleomagnetic Field 145*, pp. 221–232, eds Channell, J.E.T., Kent, D.V., Lowrie, W. & Meert, J.G., American Geophysical Union, Washington, D.C.
- Coe, R.S. & Prévot, M., 1989. Evidence suggesting extremely rapid field variation during a geomagnetic reversal, *Earth planet. Sci. Lett.*, **92**, 292–298, doi:10.1019/0012-821X(89)90053-8.
- Coe, R.S., Prévot, M. & Camps, P., 1995. New evidence for extraordinarily rapid change of the geomagnetic field during a reversal, *Nature*, **374**, 687–692.
- Coe, R.S., Hongre, L. & Glatzmaier, G.A., 2000. An examination of simulated geomagnetic reversals from a palaeomagnetic perspective, *Phil. Trans. R. Soc. Lond. A.*, **358**, 1141–1170.
- Cogne, J.P., 2003. PaleoMac: a Macintosh TM application for treating paleomagnetic data and making plate reconstructions, *Geochem. Geophys. Geosyst.*, **4**, doi:10.1029/2001GC000227.
- Colgan, J.P., Dumitru, T.A., McWilliams, M. & Miller, E.L., 2006. Timing of Cenozoic volcanism and Basin and Range extension in northwestern Nevada: new constraints from the northern Pine Forest Range, *Geol. Soc. Am. Bull.*, **118**, 126–139.
- Cox, A., 1968. Lengths of geomagnetic polarity intervals, *J. geophys. Res.*, **73**, 3247–3260.
- Cox, A., 1969. Confidence limits for the precision parameter K, *Geophys. J. R. astr. Soc.*, **18**, 545–549.
- Enkin, R., 2005. *PMGSC 4.2*, Geological Survey of Canada, Sidney, British Columbia.
- Fisher, R.A., 1953. Dispersion on a sphere, *Proc. R. Soc. Lond. A*, **217**, 295–305.
- Fuller, R.E., 1931. *The Geomorphology and Volcanic Sequence of Steens Mountain in Southeastern Oregon*, Univ. Washington Pub. Geol. Vol. 3, No. 1, University of Washington Press, Seattle, WA, 130pp.
- Glatzmaier, G.A., Coe, R.S., Hongre, L. & Roberts, P.H., 1999. The role of the Earth's mantle in controlling the frequency of geomagnetic reversals, *Nature*, **401**, 885–890.
- Glen, J.M.G., Coe, R.S. & Liddicoat, J.C., 1999. A detailed record of paleomagnetic field change from Searles Lake, California. 2. The Gauss/Matuyama polarity reversal., *J. geophys. Res.*, **104**, 12 883–12 894.
- Goldstein, M.A., Strangway, D.W. & Larson, E.E., 1969. Paleomagnetism of a Miocene Transition Zone in Southeastern Oregon, *Earth planet. Sci. Lett.*, **7**, 231–239.
- Gradstein, F., Ogg, J. & Smith, A., 2004. *A Geologic Time Scale*, Cambridge University Press, Cambridge, 589pp.
- Grand, S.P., 2002. Mantle shear-wave tomography and the fate of subducted slabs, *Phil. Trans. R. Soc.*, **360**, 2475–9461.
- Hagstrum, J.T. & Champion, D.E., 2002. A Holocene paleosecular variation record from 14C-dated volcanic rocks in western North America, *J. geophys. Res.*, **107**, doi:10.1029/2001JB000524.
- Herber-Bervera, E. & Coe, R.S., 1999. Transitional field behaviour during the Gilbert-Gauss and lower Mammoth reversals recorded in lavas from the Wai'anae Volcano, O'ahu, Hawaii, *J. geophys. Res.*, **104**, 29 157–29 173.
- Hoffman, K.A., 1992. Dipolar reversal states of the geomagnetic-field and core mantle dynamics, *Nature*, **359**, 789–794.
- Hoffman, K.A., Singer, B.S., Camps, P., Hansen, L.N., Johnson, K.A., Clipperton, S. & Carvallo, C., 2008. Stability of mantle control over dynamo flux since the mid-Cenozoic, *Phys. Earth planet. Int.*, **169**, 20–27.
- Hooper, P.R., Binger, G.B. & Lees, K.R., 2002. Ages of the Steens and Columbia River flood basalts and their relationship to extension-related calc-alkalic volcanism in eastern Oregon, *Geol. Soc. Am. Bull.*, **114**, 43–50.
- Hooper, P.R., Camp, V.E., Reidel, S.P. & Ross, M.E., 2007. The origin of the Columbia River flood basalt province: plume versus nonplume models, in *Plates, Plumes and Planetary Processes 430*, pp. 635–668, eds Foulger, G.R. & Jurdy, D.M., Geological Society of America, Boulder, CO.
- Jarboe, N.A., Coe, R.S., Renne, P.R., Glen, J.M.G. & Mankinen, E.A., 2008. Quickly erupted volcanic sections of the Steens Basalt, Columbia River Basalt Group: secular variation, tectonic rotation, and the Steens Mountain reversal, *Geochem. Geophys. Geosyst.*, **9**, doi:10.1029/2008GC002067.
- Jarboe, N.A., Coe, R.S., Renne, P.R. & Glen, J.M.G., 2010. The age of the Steens reversal and the Columbia River Basalt Group, *Chem. Geol.*, **274**, 158–168.
- Kirschvink, J.L., 1980. The least-squares line and plane and the analysis of paleomagnetic data, *Geophys. J. R. astr. Soc.*, **62**, 699–718.
- Korte, M. & Constable, C.G., 2005. Continuous geomagnetic field models for the past 7 millennia: 2. CALS7K, *Geochem. Geophys. Geosyst.*, **6**, doi:10.1029/2004GC000800.
- Kutzner, C. & Christensen, U.R., 2004. Simulated geomagnetic reversals and preferred virtual geomagnetic pole paths, *Geophys. J. Int.*, **157**, 1105–1118.
- Laj, C., Mazaud, A., Weeks, R., Fuller, M. & Herrerobervera, E., 1991. Geomagnetic reversal paths, *Nature*, **351**, 447–447.
- Langereis, C.G., Vanhoof, A.A.M. & Rochette, P., 1992. Longitudinal confinement of geomagnetic reversal paths as a possible sedimentary artifact, *Nature*, **358**, 226–230.
- Leonhardt, R. & Fabian, K., 2007. Paleomagnetic reconstruction of the global geomagnetic field evolution during the Matuyama/Brunhes transition: iterative Bayesian inversion and independent verification, *Earth planet. Sci. Lett.*, **253**, 172–195.

- Leonhardt, R., McWilliams, M., Heider, F. & Soffel, H.C., 2009. The Gilsa excursion and the Matyuma-Brunhes transition recorded in ^{40}Ar - ^{39}Ar dated lavas from Lanai and Maui, Hawaiian Islands, *Geophys. J. Int.*, **179**, 43–58.
- Love, J.J., 1998. Paleomagnetic volcanic data and geometric regularity of reversals and excursions, *J. geophys. Res.*, **103**, 12435–12452.
- Love, J.J., 2000. Statistical assessment of preferred transitional VGP longitudes based on palaeomagnetic lava data, *Geophys. J. Int.*, **140**, 211–221.
- Love, J.J. & Mazaud, A., 1997. A database for the Matayama–Brunhes magnetic reversal, *Phys. Earth planet. Int.*, **103**, 207–245.
- Magill, J. & Cox, A., 1980. *Tectonic Rotation of the Oregon Western Cascades: Oregon Department of Geology and Mineral Industries Special Paper 10*, Oregon Department of Geology and Mineral Industries, Oregon, 67pp.
- Magill, J. & Cox, A., 1981. Post-oligocene tectonic rotation of the Oregon Western Cascade Range and the Klamath Mountains, *Geology*, **9**, 127–131.
- Mankinen, E.A., Prévot, M., Grommé, C.S. & Coe, R.S., 1985. The Steens Mountain (Oregon) geomagnetic polarity transition. 1. Directional history, duration of episodes, and rock magnetism, *J. geophys. Res.*, **90**, 10393–10416.
- Mankinen, E.A., Larson, E.L., Grommé, C.S., Prévot, M. & Coe, R.S., 1987. The Steens Mountain (Oregon) geomagnetic polarity transition. 3. Its regional significance, *J. geophys. Res.*, **92**, 8057–8076.
- McCaffrey, R., *et al.*, 2007. Fault locking, block rotation and crustal deformation in the Pacific Northwest, *Geophys. J. Int.*, **169**, 1315–1340.
- McFadden, P.L. & McElhinny, M.W., 1988. The combined analysis of remagnetization circles and direct observations in paleomagnetism, *Earth planet. Sci. Lett.*, **87**, 161–172.
- McFadden, P.L. & McElhinny, M.W., 1995. Combining groups of paleomagnetic directions or poles, *Geophys. Res. Lett.*, **22**, 2191–2194.
- Minor, S. A., 1986. Stratigraphy and structure of the Western Trout Creek and Northern Bilk Creek Mountains, *MSc thesis*, University of Colorado, Harney County, OR and Humboldt County, NV.
- Morris, E.R., Schillinger, W., Coe, R.S., Pluhar, C.J. & Jarboe, N.A., 2009. Automating the 2G superconducting rock magnetometer for single-solenoid alternating field demagnetization, *Geochem. Geophys. Geosyst.*, **10**, doi:10.1029/2008GC002289.
- Ohno, M. & Hamano, Y., 1992. Geomagnetic poles over the past 10000 years, *Geophys. Res. Lett.*, **19**, 1715–1718.
- Olson, P. & Christensen, U.R., 2002. The time-averaged magnetic field in numerical dynamos with non-uniform boundary heat flow, *Geophys. J. Int.*, **151**, 809–823.
- Prévot, M. & Camps, P., 1993. Absence of preferred longitude sectors for poles from volcanic records of geomagnetic reversals, *Nature*, **366**, 53–57.
- Prévot, M., Mankinen, E.A., Coe, R.S. & Grommé, C.S., 1985. The Steens Mountain (Oregon) geomagnetic polarity transition. 2. Field intensity variations and discussion of reversal models, *J. geophys. Res.*, **90**, 10 417–10 488.
- Quidelleur, X. & Valet, J.P., 1996. Geomagnetic changes across the last reversal recorded in lava flows: from La Palma, *Canary Islands*, **101**, 13 755–13 773.
- Schnepf, E. & Lanos, P., 2005. Archaeomagnetic secular variation in Germany during the past 2500 years, *Geophys. J. Int.*, **163**, 479–490.
- Singer, B.S., Relle, M.K., Hoffman, K.A., Battle, A., Laj, C., Guillou, H. & Carracedo, J.C., 2002. Ar/Ar ages from transitionally magnetized lavas on La Palma, Canary Islands, and the geomagnetic instability timescale, *J. geophys. Res.*, **107**, 2307 doi:10.1029/2011JB001613.
- Torsvik, T.H., Muller, R.D., Van der Voo, R., Steinberger, B. & Gaina, C., 2008. Global plate motion frames: toward a unified model, *Rev. Geophys.*, **46**, doi:10.1029/2007RG000227.
- Tric, E., Laj, C., Jehanno, C., Valet, J. P., Kissel, C., Mazaud, A. & Iaccarino, S., 1991. High-resolution record of the upper Olduvai transition from Po Valley (Italy) sediments—support for dipolar transition geometry, *Phys. Earth planet. Int.*, **65**, 319–336.
- Valet, J.P. & Plenier, G., 2008. Simulations of a time-varying non-dipole field during geomagnetic reversals and excursions, *Phys. Earth planet. Int.*, **169**, 178–193.
- van Hoof, A.A.M. & Langereis, C.G., 1991. Reversal records in Marine Marls and delayed acquisition of remanent magnetization, *Nature*, **351**, 223–225.
- Watkins, N.D., 1965. Frequency of extrusions of some Miocene Lavas in Oregon during an apparent transition of the polarity of the geomagnetic field, *Nature*, 801–803.
- Watkins, N.D., 1969. Non-dipole behaviour during an upper Miocene geomagnetic polarity transition in Oregon, *Geophys. J. R. astr. Soc.*, **17**, 121–149.

SUPPORTING INFORMATION

Additional Supporting Information may be found in the online version of this article:

Photos. A selection of photos of the Catlow, Poker Jim South A and B and Steens B sections.

Please note: Wiley-Blackwell is not responsible for the content or functionality of any supporting materials supplied by the authors. Any queries (other than missing material) should be directed to the corresponding author for the article.